Prepared for submission to JCAP

Universality of the halo mass function in screened gravity theories

F. von Braun-Bates,[a,1] **and J. Devriendt**[a,b]

[a]Astrophysics, University of Oxford, Denys Wilkinson Building, Keble Road, Oxford OX1 3RH, UK

[a,b]Observatoire de Lyon, UMR 5574, 9 avenue Charles Andre, F-69561 Saint Genis Laval, France

E-mail: francesca.vonbraun-bates@physics.ox.ac.uk, julien.devriendt@physics.ox.ac.uk

Abstract. We examine the efficacy of the halo mass function as a probe of $f(\mathcal{R})$, symmetron and DGP gravity. We develop an excursion-set method to generalise a range of popular HMF fitting functions from GR to screened MG, considering the HMF dependence on the critical density parameter δ_c. In particular, we propose a variety of new methods to account for the environmental dependence of chameleon screening and compare their accuracy to existing ones via N-body data. Finally, using the nested sampling routine `MultiNest`, we examine two possible interpretations of the MG N-body results: whether they can be interpreted as ΛCDM HMFs and whether the MG HMFs display any universality.

We find that the effects of MG can be interpreted as a change in best-fit parameters in the ΛCDM HMF—i.e. can be mistaken for GR—for all of the fitting functions. Alternatively, the relation can be inverted to judge the universality of the HMF—not in terms of its purported invariance to z, H_0, Ω_m, Ω_Λ as in GR, but its independence on the underlying theory of gravity. Although we found no completely universal HMF, the parameter values did cluster according to the type of screening mechanism. The results suggest that a single, best-fit HMF might be used for each type of screening, independent of the parameters in the MG model. This demonstrates that the additional complexity of the gravitational collapse in screened MG theories cannot always be accounted for using the techniques developed in GR. However, the variations are small enough that it is unnecessary to develop new fitting functions and calibrate them on a case-by-case basis.

[1]Corresponding author.

Contents

1 Introduction

The halo mass function (HMF) $n(M)dM$ is the number n of haloes with mass in the range $[M, M + dM]$ per unit volume. It has two remarkable properties which render it a useful probe of extensions to general relativity (GR). On the one hand, it is (nearly-)universal, in the sense that it can be written in a form $f(\nu)$ which is (practically) insensitive to changes in redshift and cosmological parameters [1, 2], where ν is the universal parameter and f is a fitting function with a number of free parameters. On the other hand, the HMF is sensitive to both the expansion history of the universe and the nonlinear behaviour of spherical collapse via the critical density parameter δ_c [3] and the matter power spectrum via the halo resolution $S(M)$ (both of which appear in ν). This presents a number of interesting possibilities for the use of the HMF in modified or extended gravity theories, namely:

- How do underlying assumptions in constructing the HMF from simulations affect the success of the fitting functions?
- Should we blindly apply HMFs calibrated using GR (specifically ΛCDM) to other theories of gravity?
- Can evidence for modifications to GR be mistaken for changes in the free parameters in the GR HMF?
- Which HMFs are more universal across (i.e. insensitive to) different gravity theories?
- Do the extra gravitational degrees of freedom necessitate additional free parameters in the HMF?

Only after such avenues are investigated can we begin to probe the universality of the HMF in MG theories. We cannot determine whether the kind of universality of the HMF enjoyed in GR also applies to extended gravity theories without understanding its behaviour at a fixed redshift and cosmology. This paper addresses all of these questions for a comprehensive range of currently-viable HMFs by focusing on a subset of MG theories known as screened gravity.

Modifications to GR are motivated by a number of factors. From a theoretical standpoint, it is interesting to see what extensions to GR are permitted by Lovelock's theorem [4]. From a cosmological viewpoint, the era of precision cosmology now enables us to distinguish between competing gravitational models. While the concordance cosmology of ΛCDM has performed remarkably well over the past two decades [5], there exist theoretical problems[1] and tensions between observations measured at early and late times.[2] Thus it is useful to have a range of possible gravity models which may alleviate these problems. Clearly, these motives give rise to a plethora of theories (e.g. [4]), and it is impractical to test them all. Therefore in this paper we restrict ourselves to Hu & Sawicki-$f(\mathcal{R})$, Symmetron and Dvali-Gabadadze-Porrati (DGP) gravity. This selection represents a range of MG families and screening mechanisms, while ensuring that each theory is sufficiently related to take a unified approach.

A pre-requisite for using the HMF as a probe of MG is a firm understanding of its behaviour in GR. Superficially this may be obvious: the analytical HMF of Press and Schechter [7] has long been supplanted by a range of fitting functions (summarised in e.g. [8]) whose free parameters are calibrated using N-body simulations. This calibration is valid only for certain cosmological parameters (which were employed in the N-body code) and a certain range in mass and redshift (for which the fit agrees with the simulation bins). It is this fitting function $f(\nu)$ which is universal—in the sense that that $f(\nu)$ can be applied to a range of redshifts and cosmologies [9]—rather than the HMF itself $n(M)$. Recently, there has been disagreement over whether [1, 10, 11] or not [12–14] this universality holds—and even these papers test only a few of the competing fitting functions. Despite this, once various obscuring factors are addressed, the deviations from non-universality in the calibrated HMFs are of a few percent [9]. In particular, if one uses the correct measurement of halo over-density [15] and includes z-dependence in the over-density and the resolution, the best-fit parameter

[1] Examples include fine-tuning of Λ, the lack of direct detection of CDM, possible fine-tuning of inflation [4].

[2] Compare measurements with Planck 2015 [6] to the values of σ_8 from weak lensing and cluster number counts, H_0 from Lyman-α measurements of BAO, $f\sigma_8$ from redshift-space distortions [5].

values provide an HMF which applies over several decades of mass and beyond $z = 0$ (sometimes up to $z = 30$; [12]), but only for a fixed cosmology [16]. Thus, we can firmly establish the null result against which to test the effects of modified gravity.

The mechanism for generating halo mass functions differs in the MG and GR cases. Due to the additional computation time and complexity required to run N-body simulations (discussed in Section 4.1), in MG one cannot take the GR approach of the previous paragraph. Instead, one typically uses either the Press-Schechter or the Sheth-Tormen functions (although [17] uses the Peacock function). However, there appears to be little consensus on how the fifth-force degree of freedom affects the suitability of the fitting functions. Some authors use the Sheth-Tormen fit on the grounds that this is considered satisfactory in the GR simulations (symmetron [18], $f(\mathcal{R})$ [19], DGP [20]). A counter-example is the Galileon HMF: the authors of [21] reason that the assumptions used in the Sheth-Tormen model are unlikely to hold, given the Galileon fifth-force modification to GR, and so use the Press-Schechter fit. It is worth noting that both DGP and Galileon theories fall into the broader class of Vainshtein mechanism models—so in some sense the modification to gravity is the same—yet there is no agreement on which excursion set model is the appropriate one. The $f(R)$ mass function is relatively advanced in comparison, with a variety of different approaches [17, 19, 22, 23] in reasonable agreement. The process of deriving the MG HMF highlights ambiguities in the universal parameter $\nu = \delta_c/\sqrt{S}$ which are not present in GR: do we change only $S(M)$ [23] or only δ_c [17] or both [19], or do we need to evolve the full scalar field equations [22]? Once we have defined ν, what should be done about the parameter values? Usually the ΛCDM values are retained; sometimes the normalisation constant is left free while the other parameters are fixed at ΛCDM values [18] or recalibrated from appropriate MG simulations [24, 25]. These approaches illustrate the additional theoretical and practical complications when deriving an appropriate HMF in modified gravity.

This paper seeks to address these issues. First we outline the various screened models of MG used in this paper in Section 2. More detail is provided on: $f(R)$ in Appendix A.1, Symmetron in Appendix A.2 and DGP in Appendix A.3. Then Section 3 summarises the fitting functions used in this paper and why they are universal, before generalising the MG HMFs from their GR equivalent. Next we describe the numerical work: Section 4.1 outlines the simulation parameters and algorithms used for the various N-body simulations and the extraction of the HMF from the simulations; Section 5 outlines the theory used to calculate the best-fit values for the free parameters in the HMFs. (We calibrate the "nested sampling" algorithm and describe the data processing effects in Appendix B). The results section discusses the questions raised at the beginning of this paper: Section 6.2 shows how MG manifests in the parameters even when assuming a ΛCDM HMF; Section 6.3 recalibrates the fitting functions using the same gravity model in both the N-body simulations and the HMFs. Finally we summarise our method and key results in Section 7.1 and discuss avenues for further work in Section 7.2.

The conventions used throughout this paper are:

- Units $c = 1$, Einstein constant $\kappa = 8\pi G/c^2$, Planck mass $M_{Pl} = \kappa^{-1/2}$
- Gauge choice is conformal Newtonian with metric signature $(-+++)$

$$\mathrm{d}\, s^2 = a^2(\tau)\left[-(1+2\Psi)\,\mathrm{d}\,\tau^2 + (1-2\Phi)\delta_{ij}\,\mathrm{d}\,x^i\,\mathrm{d}\,x^j\right]$$

- The full spacetime metric has Greek indices ranging from 0 to 3 while flat spatial hypersurfaces have Roman indices ranging from 1 to 3.

This accounts for a variety of sign changes in some formulae compared to the equations in the citations.

2 Screened gravity theories

The MG theories studied in this paper share a common trait to ensure that the successes of GR are unaffected by any modifications. The *screening mechanism* is a technique whereby fifth-force modifications to GR are "screened away" in regions where the theory must mimic GR in order to be experimentally viable. A range of such techniques exists, so we limit ourselves to three popularly-held categories of screening—*chameleon* [26], *symmetron* [27, 28] and *Vainshtein* [29]—by selecting one theory from each family, namely: Hu & Sawicki $f(\mathcal{R})$ ([30]; chameleon), Hinterbichler-Khoury symmetron [27] and Dvali-Gabadadze-Porrati ([31]; Vainshtein). Our parameter values are tabulated in Table 2.

The background evolution of these models is always close to ΛCDM for viable values of the free parameters. Accordingly, we only employ the MG modification in computing the spherical collapse of the haloes within a ΛCDM background.

The effect of the scalar field in the halo model is just a redefinition of the Poisson equation. Sufficient conditions are that we apply the weak-field, quasi-static limit to the perturbed field equations and the equation of motion of the scalar field: after copious algebra [32] show that this relates the metric perturbations Φ, Ψ to the perturbed field χ and gauge-invariant matter density δ. More algebraic manipulation allows us to recast this as a Poisson equation (for details see [32]). Thus we obtain our effective multiplication of $G_{\rm eff} = (1 + F_{\rm eff})G_N$. The different MG models explored in this paper are summarised in Table 2.

Let us characterise the various types of screening used in this paper. Screening mechanisms add new terms to the GR action, which are designed to suppress the non-GR modi-

MG model	Ref.	Screening	$F_{\rm eff}$	Parameter values
$f(R)$	[30]	chameleon	Eqn. A.3	$\lvert f_{R0}\rvert = 10^{-5}, 10^{-6}$ $n_{f(R)} = 1$
Symmetron	[27]	symmetron	Eqn. A.4	$\lambda = 1$ Mpc$/h$ $\beta_0 = 1$ $a_{\rm SSB} = 0.33, 0.5$
DGP	[31]	Vainshtein	Eqn. A.6	$r_c = 1.2, 5.6$ c/H$_0$

Table 2: The various gravity models used throughout this paper.

fications under certain conditions. By construction, this suppression of the fifth-force modification happens on non-linear regimes. The conditions required for screening divide the mechanism into three groups: chameleon, symmetron and Vainshtein. The different screening methods correspond to different behaviours of the Lagrangian, which we can classify by expanding about some value ϕ_0 by an infinitesimal value $(\delta\phi)$ [33]:

$$\mathcal{L} = \frac{1}{2}\mathcal{R}M_{\rm Pl}^2 + \partial_\mu(\delta\phi)\,\partial_\nu(\delta\phi)\,Z^{\mu\nu}(\phi_0) + (\delta\phi)\,m^2(\phi_0) + \frac{\rho_m}{M_{\rm Pl}}\beta(\phi_0) \tag{2.1}$$

In low density regions the scalar field takes a value $\phi_0 = \phi_{\rm low}$, for which:@

$$\gamma \equiv \left|\frac{\vec{F}_\phi}{\vec{F}_N}\right| \propto \beta^2(\phi_{\rm low}) \sim 0 \tag{2.2}$$

and we see that the contribution of the fifth force $|\vec{F}_\phi|$ is non-negligible compared to the Newtonian value $|\vec{F}_N|$. Compare this to the high-density value $\phi_0 = \phi_{\rm high}$, for which:

$$\gamma \ll 1 \qquad \text{by definition} \tag{2.3a}$$

which can only be produced by:

$$\beta(\phi_{\rm high}) \ll \beta(\phi_{\rm low}) \qquad \text{matter coupling suppressed} \qquad \text{(symmetron)} \tag{2.3b}$$

$$m(\phi_{\rm high}) \gg m(\phi_{\rm low}) \qquad \text{large local mass} \qquad \text{(chameleon)} \tag{2.3c}$$

$$Z^{\mu\nu}(\phi_{\rm high}) \gg Z^{\mu\nu}(\phi_{\rm low}) \qquad \text{weakened matter source} \qquad \text{(Vainshtein)} \tag{2.3d}$$

This permits us to classify a screened MG theory not by abstract considerations (*i.e.* which conditions are relaxed in Lovelock's Theorem) but rather by the practicalities of the mechanism by which it evades local tests of gravity.

Appendix A provides more detail on the fifth-force modification caused by various MG theories used in this paper. We have already demonstrated how to use the effective fifth-force contribution to G to find the density required for collapse of a spherical top-hat in [17]. We now turn our attention to the halo mass functions in the next section.

3 Generalising the halo mass function from GR to MG

The halo mass function $n(M)$ is defined to be the number density of dark matter haloes in a given mass interval at a certain redshift. Using excursion set theory, this can be related to the probability $f(S)$ for a given trajectory in the phase space (δ, S) to be absorbed at resolution S when the over-density δ reaches the collapse density δ_c. This behaviour amounts to a diffusion equation, where δ and S act as spatial and temporal variables respectively. In turn, $f(S)$ can be expressed in terms of a "universal" fitting function $F(\nu)$, which is invariant under changes in redshift and cosmological parameters. The same method can be used for empirical fitting functions, which are derived from and calibrated using N-body simulations. In particular we focus on the various ways to account for environment dependence—a problem peculiar to chameleon MG theories—and in Section 6.1 we analyse the accuracy of both existing methods and the novel methods which we propose in this paper.

This section summarises the various halo mass functions used in this paper. In GR a variety of empirical fits to N-body simulations have been proposed in a "universal" form

Cosmology	Parameters				HMF paper(s)
	Ω_{m0}	$\Omega_{\Lambda 0}$	σ_8	h	
ΛCDM	0.269	0.731	0.80	0.704	This paper
	0.29	0.71	0.90	0.72	WMAP1 (Courtin)
	0.30	0.70	0.90	0.70	WMAP1 (Sheth-Tormen, Jenkins, Tinker, Warren)
	0.24	0.76	0.74	0.73	WMAP3 (Courtin, Reed)
	0.24	0.76	0.75	0.73	WMAP3 (Tinker)
	0.24	0.76	0.8	0.73	WMAP3 (Tinker)
	0.26	0.74	0.79	0.72	WMAP5 (Courtin)
	0.27	0.73	0.80	0.70	WMAP5 (Watson)
	0.28	0.72	0.80	0.70	WMAP5 (Watson)
	0.27	0.73	0.90	0.70	
	0.27	0.73	0.79	0.70	
	0.26	0.74	0.75	0.71	Tinker
	0.23	0.77	0:75	0:73	
	0.20	0.80	0:90	0:70	
	0.25	0.75	0.80	0.70	Crocce
	0.25	0.75	0.80	0.73	Peacock
	0.25	0.75	0.90	0.73	Angulo, Reed
SCDM	1.0	0.0	0.60	0.50	Sheth-Tormen
	1.0	0.0	0.51	0.50	Jenkins
	1.0	0.0	0.79	0.72	Courtin
OCDM	0.30	0.0	0.85	0.70	Sheth-Tormen, Jenkins
τCDM	1.0	0.0	0.51	0.5	Jenkins
	1.0	0.0	0.60	0.50	Sheth-Tormen, Jenkins
L-ΛCDM	0.10	0.90	0.79	0.72	Courtin
LRP-CDM	0.26	0.74	0.79	0.72	Courtin

Table 3: Cosmological parameters used to derive each of the HMF fitting functions in GR.

$f(\nu)$. The aim of these fits is to find a fitting function over a broad range of masses which is independent of redshift and cosmology, and the extent to which each fitting function exhibits this universality is a controversial one even in GR. Nonetheless, we show how to generalise the HMFs proposed in GR to three types of screened MG. Furthermore, we show a variety of methods to include environment dependence in the HMF, as required by chameleon-screened MG. A summary of the functions used in this paper is in Table 4.

Two of the fitting functions used here (*viz.* Press-Schechter and Sheth-Mo-Tormen) can be derived analytically. The Press-Schechter function results from assuming spherical symmetry and a flat (scale-independent) barrier density. That Press-Schechter can be derived analytically in screened MG (e.g. for a chameleon model [34]) via a simple change of variables is the very reason that we can extend the other mass functions in this paper to MG as well.

The Sheth-Mo-Tormen function in [35, 36] was originally a fit to data with the substitution $\delta_c \to \sqrt{a}\delta_c$ made to produce a better fit than Press-Schechter. Later [37] showed that this is equivalent to using excursion set theory with the moving barriers which result from ellipsoidal collapse. To our knowledge, no-one has shown that the assumptions used to construct the Sheth-Tormen function in GR also hold in MG. Nonetheless, the analyticity in GR makes these appealing functions for use in MG.

The remaining fitting functions are purely empirical fits, derived from ΛCDM N-body simulations. Having extracted the discrete approximation to the HMF $n(M)$, this can be converted to a discrete first-crossing distribution and a continuous "best-fit" approximation found—either in terms of σ or in terms of ν—which holds for a given redshift (range), mass range and cosmology (or family of cosmologies). The resulting HMF also depends upon the halo finder used to extract the halo masses, as well as any subsequent calibration or corrections. These factors all contribute to the final parameter values adopted by a particular function. This is particularly notable for the Sheth-Mo-Tormen fit, for which several authors[3] [13, 16, 35, 38] have proposed their own "improved" values for the best-fit parameters of this function. This emphasises that while the same functional form can provide a good fit to data in different background cosmologies, the same N-body data and the same fitting function will produce different best-fit parameters and varying degrees of invariance depending upon the halo extraction tehcniques and the theoretical assumptions of the authors. For this reason, we have separated the HMFs into families which share the same functional form. We summarise the HMFs $f(\nu)$ in Table 4.

There are four steps involved in generalising the ΛCDM HMFs to MG:

1. Calculating the appropriate barrier density;
2. Selecting the appropriate linearised power spectrum;
3. Converting from σ to ν as the dependent variable;
4. Rescaling the free parameters accordingly.

[3]This is why Jenkins appears twice in Table 4: one instance is their calibration for the SMT function (as with Courtin) and the other is their new fitting function.

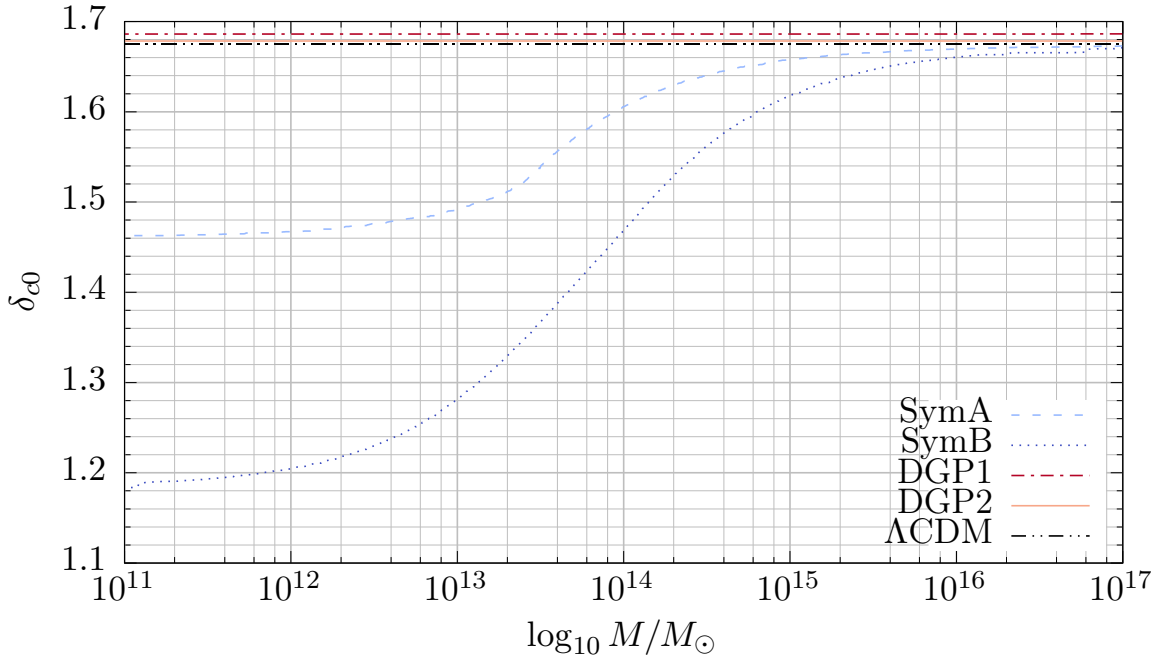

(a) DGP $r_c = 1.2c/H_0$, DGP $r_c = 5.6c/H_0$, Symmetron $a_{\rm SSB} = 0.5$, Symmetron $a_{\rm SSB} = 0.33$

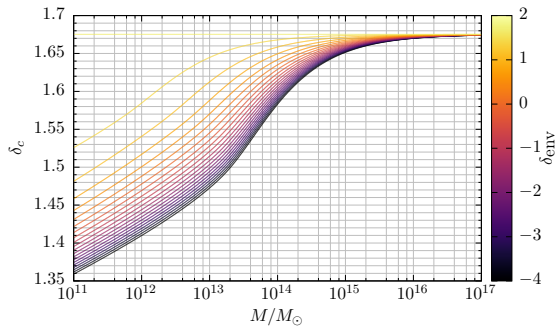

(b) $|f_{\mathcal{R}0}| = 10^{-6}$

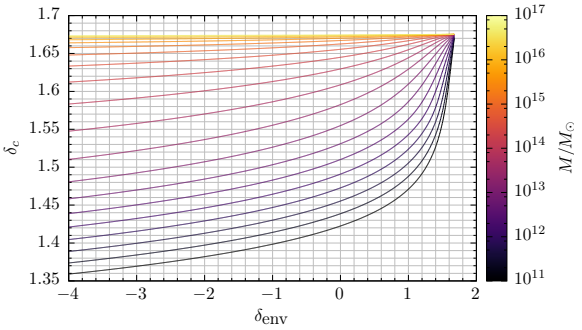

(c) $|f_{\mathcal{R}0}| = 10^{-6}$

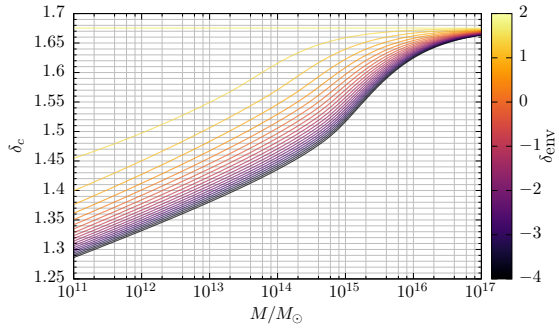

(d) $|f_{\mathcal{R}0}| = 10^{-5}$

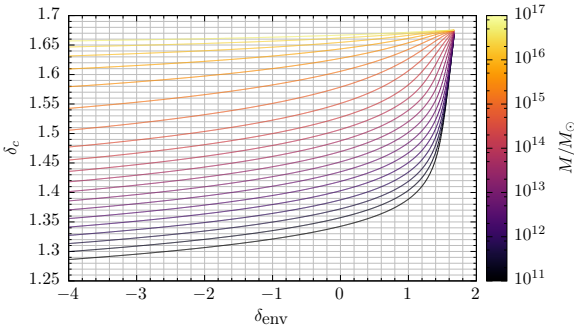

(e) $|f_{\mathcal{R}0}| = 10^{-5}$

Figure 1: The barrier density $\delta_c(M, \delta_{\rm env})$ for each of the MG models in this paper.

We discussed Item 1 in [17]. The barrier densities for the models in this paper are in Figure 1.

In Item 2 we must decide whether to keep the ΛCDM power spectrum or to adjust it according to the MG theory. We keep the linear $P(k)$ from ΛCDM, in agreement with [17, 39].

Item 3 is concerned with making explicit the dependence on the collapse density. In GR, one is faced with the question of whether the appropriate independent variable for the HMF is ν or S (equivalently any other function of σ). Those in the former camp (*inter alia* [1, 35, 36, 40]) assert that according to excursion set theory the (albeit weak) cosmological and redshift dependence of both δ_c and σ cancel when the first-crossing distribution is expressed in terms of $\nu \equiv \delta_c/\sigma$ in GR cosmologies. Those in the latter camp (*inter alia* [9, 12–14, 38, 41]) assert that δ_c is a sufficiently weak function of Ω_{m0} and z that this dependence can be ignored; in fact [38] go so far as to say that "taking $\delta_c = 1.686$ in all cosmologies leads to excellent agreement with our numerical data if halos are defined at fixed over-density". Thus, while the choice of S or ν appears to be mere semantics in GR cosmologies (because this is an invertible mapping if and only if δ_c is assumed to be a constant), this is clearly not the case in our extended gravity theories. This is especially true for $f(\mathcal{R})$, which has both a mass- and $\delta_{\rm env}$-dependence for δ_c.

Item 4 is the consequence of Item 3. All the free parameters in the HMFs[4] need to be converted from $\ln\left(\sigma^{-1}\right)$ to ν, by absorbing factors of δ_c. This requires paying particular attention to whether the SCDM or ΛCDM collapse density is used in the original papers, as this has implicitly been absorbed into the best-fit parameters.[5] This "updates" the ΛCDM-calibrated fits to a format which is compatible both with GR and MG.

This is sufficient for MG theories which only have a drifting barrier $\delta_c(S)$, but not for the drifting-and-diffusing barrier $\delta_c(S, \delta_{\rm env}, S_{\rm env})$. We treat this additional generalisation in the next few paragraphs.

The drifting-and-difffusing barrier can be accounted for using a wide variety of methods:

1. Scaling using the Volterra integral solution in Equation (3.1a)

2. Averaging over the cosmic web (described in [17])

3. Calculating a $\delta_{\rm env}$-averaged collapse density, i.e. converting to a drifting barrier

4. A flat or linear-barrier approximation to the full excursion-set problem

We address each of these in turn.

Technique 1 utilises the fact that we already know how to account for the extra barrier complexity in the excursion set approach: whereas the flat barrier produces the Press-Schechter distribution, the drifting-and-diffusing barrier leads to an integral equation given

[4]The "Reed 2007" fit is the 2003-like fit from [12], rather than the one with $n_{\rm eff}(\sigma)$ dependence, which creates ambiguity about which terms to convert to ν. In the fit we use the σ-dependence is clearly only caused by treating δ_c as a constant.

[5]If we were concerned with redshift evolution, we would have to decide whether to absorb δ_{c0} or $\delta_c(z)$. Some authors fix δ_c and allow the free parameters to vary with redshift; others do the opposite.

in [42, 43]:

$$f(S|S_{\rm env},\delta_{\rm env}) = g(S) + \int_{S_{\rm env}}^{S} \mathrm{d}\,x\; k(S,x)\, f\left(x \,|\, S_{\rm env},\delta_{\rm env}\right) \tag{3.1a}$$

$$k(S,x) = \left[\frac{\delta_c(S)-\delta_c(x)}{S-x} - 2\frac{\mathrm{d}\,\delta_c(S)}{\mathrm{d}\,S}\right] \frac{1}{\sqrt{2\pi(S-x)}} \exp\left\{-\frac{(\delta_c(S)-\delta_c(x))^2}{2(S-x)}\right\} \tag{3.1b}$$

$$g(S) = \left[\frac{\delta_c(S)-\delta_{\rm env}}{S-S_{\rm env}} - 2\frac{\mathrm{d}\,\delta_c(S)}{\mathrm{d}\,S}\right] \frac{1}{\sqrt{2\pi(S-S_{\rm env})}} \exp\left\{-\frac{(\delta_c(S)-\delta_{\rm env})^2}{2(S-S_{\rm env})}\right\} \tag{3.1c}$$

So we may calculate the unconditional HMF, i.e. assuming ($\delta_{\rm env}=0$, $S_{\rm env}=0$), then accounting for the effects of the drifting and diffusing barrier using excursion set theory. This results in a rescaling of the unconditional HMF:

$$f(S)_{\rm MG} = f(S|S_{\rm env}=0,\delta_{\rm env}=0)_{\rm MG} \quad \frac{\text{Volterra solution}}{\text{Press-Schechter}} \tag{3.2}$$

This is efficient, as we only need to solve the Volterra equation once for each drifting-and-diffusing barrier density, rather than re-calculating for each HMF as well.

Technique 2 uses the $\nu_{\rm eff}$ prescription of [17]. This is substituted directly into the HMF:

$$\nu_{\rm eff} = \max\left\{0, \frac{\nu_h\left(S,\delta_{\rm env}\right) - \epsilon^2\left(S,S_{\rm env}\right)\nu_{\rm env}\left(S_{\rm env},\delta_{\rm env}\right)}{\sqrt{1-\epsilon^2\left(S,S_{\rm env}\right)}}\right\} \tag{3.3}$$

Since we are not interested in restricting ourselves to a particular environment, we can simplify the relevant equations in [17] to:

$$f\left(S\right) = \int_{-\infty}^{\infty} \mathrm{d}\,\nu_{\rm env}\; f\left(\nu_{\rm eff}\right) \int_{0}^{\infty} \mathrm{d}\,\rho \int_{-\rho}^{\rho} \mathrm{d}\,\theta\; p(\rho,\theta,\nu_{\rm env}) \tag{3.4}$$

We have rearranged the order of integration to highlight that the conditional mass function $f\left(\nu_{\rm eff}\right)$ is independent of ρ and θ.

Technique 3 approximates the drifting-and-diffusing barrier by a drifting-only barrier. Effectively we integrate over the environment density at the stage of calculating the collapse density:

$$\nu_{\rm eff} = \frac{\langle\delta_c\rangle_{\rm env}}{S} \quad \text{where} \quad \langle\delta_c\rangle_{\rm env} = \int_{-\infty}^{\delta_\Lambda} \mathrm{d}\,\delta_{\rm env}\; p\left(\delta_{\rm env}\,|\,S_{\rm env}\right)\; \delta_c\left(S\,|\,S_{\rm env},\delta_{\rm env}\right) \tag{3.5}$$

This effective-ν is substituted directly into the unconditional HMF. In contrast to the full barrier solution—where the random walk must upcross δ_c at S having started at $(\delta_{\rm env},S_{\rm env})$—here there is no accounting for the environment-dependent absorption of the Markovian trajectories in (δ,S) caused by the drifting-and-diffusing barrier.

The possible choices for the environment density $p\left(\delta_{\rm env}\,|\,S_{\rm env}\right)$ are the Lagrangian and Eulerian distributions. [44] have shown that the Lagrangian environment distribution can be obtained using the same excursion set method by which we have derived the PS mass function. The probability that the trajectory starting from $(0,0)$ survives to up-cross the environment density $\delta_{\rm env}$ at resolution $S_{\rm env}$ is [44]:

$$p\left(\delta_{\rm env}\right) = \frac{\mathcal{H}\left(\delta_c^\Lambda-\delta_{\rm env}\right)}{\sqrt{2\pi S_{\rm env}}}\left[\exp\left(-\frac{\delta_{\rm env}^2}{2S_{\rm env}}\right) - \exp\left(-\frac{\left(\delta_c^\Lambda-\delta_{\rm env}\right)^2}{2S_{\rm env}}\right)\right] \tag{3.6}$$

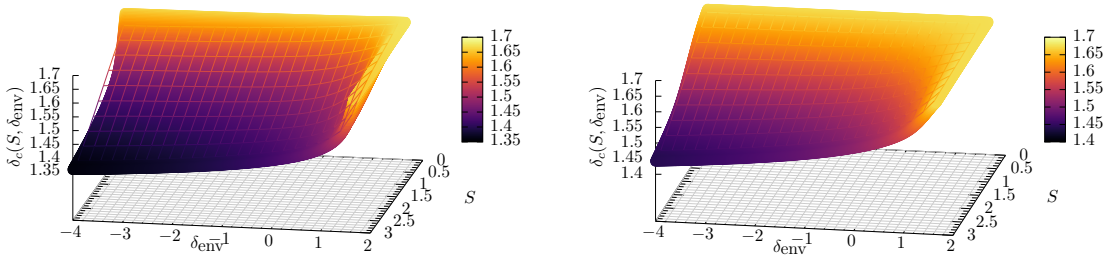

Figure 2: The full barrier (surface) and linear approximation (grid) for $f(\mathcal{R})$ models with $|f_{\mathcal{R}0}| = 10^{-5}$ and $|f_{\mathcal{R}0}| = 10^{-6}$. Both the surface and the grid are coloured according to the value of δ_c, so any areas in which the grid is visible indicate a discrepancy between the linear estimate and the true value. This is particularly pronounced for $|f_{\mathcal{R}0}| = 10^{-5}$ compared to $|f_{\mathcal{R}0}| = 10^{-6}$.

where $\delta_c^\Lambda \approx 1.676$ is the barrier density for ΛCDM and $\mathcal{H}$ is the Heaviside step function. The Eulerian distribution can be obtained from Equation (3.6) by treating the non-linear Eulerian over-density Δ as the barrier function in the excursion set method:

$$\Delta(S) = \delta_c \left[1 - \left(\frac{R_{\rm env}}{8\ {\rm Mpc}/h}\right)^{3/\delta_c} \left(\frac{S}{\sigma_8^2}\right)^{1/\omega}\right] \tag{3.7a}$$

which produces the distribution[6] for the Eulerian linear density contrast

$$q\left(\delta_{\rm env}\right) = \frac{\beta^{\omega/2}}{\sqrt{2\pi}} \left[1 + (\omega - 1)\,\frac{\delta_{\rm env}}{\delta_c^\Lambda}\right] \left[1 - \frac{\delta_{\rm env}}{\delta_c^\Lambda}\right]^{-(\omega/2+1)} \exp\left[-\frac{\delta_{\rm env}^2}{2}\left(\frac{\beta}{1 - \frac{\delta_{\rm env}}{\delta_c^\Lambda}}\right)^{\omega}\right] \tag{3.7b}$$

$$\text{where} \qquad \omega = -\delta_c \left.\frac{{\rm d}\,\ln S}{{\rm d}\,\ln M}\right|_{\rm env} \qquad \text{and} \qquad \beta = \left(\frac{R_{\rm env}}{8\ {\rm Mpc}/h}\right)^{3/\delta_c} \left(\frac{1}{\sigma_8}\right)^{2/\omega}$$

The corresponding Lagrangian and Eulerian probability density functions for $R_{\rm env} = 10\ {\rm Mpc}/h$ are shown in Figure 3.

Technique 4 approximates the full solution to the Volterra equation by a linear barrier. This is motivated by the fact that the Volterra equation with a linear barrier $\delta_c(S) = \omega - \beta S$ is calculable analytically [42]:

$$f\left(S, \delta_c(S) \,|\, S_{\rm env}, \delta_{\rm env}\right) = \frac{\delta_c - \delta_{\rm env}}{\sqrt{2\pi\left(S - S_{\rm env}\right)^3}} \exp\left[-\frac{1}{2}\frac{\left(\delta_c - \delta_{\rm env} - \beta\left(S - S_{\rm env}\right)\right)^2}{S - S_{\rm env}}\right] \tag{3.8}$$

so we can substitute the effective arguments into the fitting function, in the same way as for the cosmic web. However, Figure 2 shows that the $f(\mathcal{R})$ barriers are not linear in S (except

[6] We correct an error in [19] Equation (49) and [45] Equation (15) by restoring the $\delta_{\rm env}^2$ term in the exponent. Without it, the distribution does not normalise to unity. Furthermore [19] Equation (49) has an error in the definition of β, which is correct in [45] Equation (15).

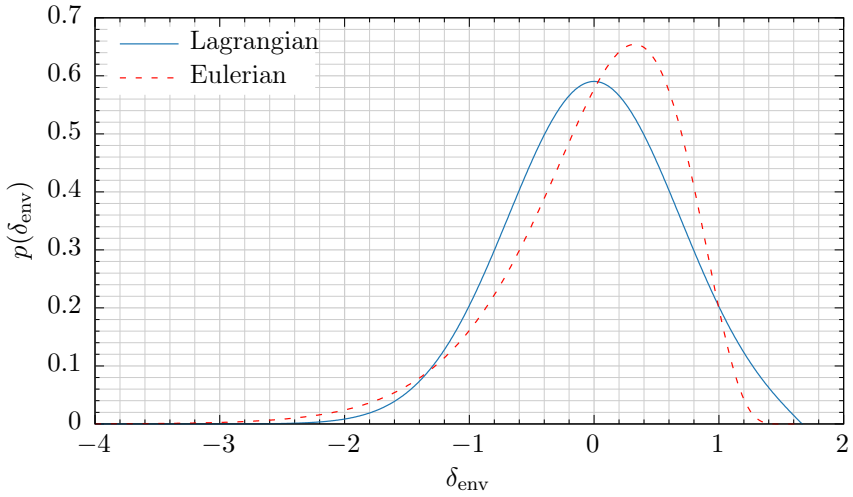

Figure 3: The probability density functions for Lagrangian and Eulerian environment density according to Equations (3.6) and (3.7b) respectively. This assumes a smoothing scale of 10 Mpc/h for both environments.

when $\delta_{\rm env} \to \delta_c^\Lambda$). The linear approximation is always an overestimate and is particularly poor at approximating the sharp rise at $\delta_{\rm env} \approx \delta_c^\Lambda$. Therefore we discard this approach due to its poor approximation.

A *caveat* for all of these methods is that there is no way to eliminate dependence on $S_{\rm env}$. The excursion set condition $S_{\rm env} < S$ prevents us from marginalising directly. The environment distributions (whether cosmic web or the PDFs for the environment overdensity) in the limit $S_{\rm env} \to 0$ do not have a finite limit. Instead we take a sufficiently large environment radius (e.g. $R_{\rm env} = 10$, 20Mpc/h) that $S > S_{\rm env}$ is always obeyed (but not too large, otherwise this is no longer a sufficiently local description of the halo surrounds [45]).

The main result of Section 6.1 is to compare these methods for generating the conditional HMFs for $|f_{\mathcal{R}0}| = 10^{-5}$ and $|f_{\mathcal{R}0}| = 10^{-6}$. For the other MG models, the barriers do not have an environment-dependent component, so their calculation is straightforward.

This updates the ΛCDM-calibrated HMFs to screened MG.

Fitting function $f(\nu)$	Mass calibration	Cosmology	Reference
$\sqrt{\frac{2}{\pi}}\nu \exp\left[-\frac{\nu^2}{2}\right]$	–	EdS	Press-Schechter [7]
$A\sqrt{\frac{2a}{\pi}}\left[1+\left(a\nu^2\right)^{-p}\right]\nu \exp\left[-\frac{a\nu^2}{2}\right]$	$\nu^2 \in [0.5, 10]$	ΛCDM SCDM OCDM	Sheth-Tormen [36]
	$\ln\sigma \in [-0.7, 0.8]$	ΛCDM, OCDM, SCDM, τCDM	Jenkins [38]
	$\ln\sigma \in [-0.7, 0.8]$	ΛCDM SCDM L-ΛCDM LRP-CDM	Courtin [16]
$A\left[\left(\frac{\nu}{\delta_c^\Lambda}\right)^a + b\right]\exp\left[-c\nu^2\right]$	$M \in [10^{10}, 10^{15}]M_\odot$	ΛCDM	Warren [13]
	$M \in [10^{10.5}, 10^{15.5}]M_\odot$	ΛCDM	Crocce [41]
$A\exp\left[-\left\|\ln\nu + b\right\|^a\right]$	$\ln\sigma \in [-1.05, 1.2]$	ΛCDM OCDM SCDM τCDM	Jenkins [38]
$\frac{\nu^2\exp(-c\nu^2)}{\left(1+a\nu^b\right)^2}\left[ab\nu^{b-1} + c(1+a\nu^b)\right]$	$M \in [10^{10}, 10^{15}]M_\odot$	ΛCDM	Peacock [40]
$A\sqrt{\frac{2a}{\pi}}\nu\exp\left[-\frac{ca\nu^2}{2}\right]$ $\left[1+\left(a\nu^2\right)^{-p} + Q\exp\left[-\frac{1}{2}\left(\frac{\ln\nu - q}{0.6}\right)^2\right]\right]$	$\ln\sigma \in [-0.9, 1.7]$	ΛCDM	Reed 2007 [12]
$A\left[(b\nu)^a + 1\right]\exp\left(-c\nu^2\right)$	$\sigma \in [10^{-0.4}, 10^{0.6}]$	ΛCDM	Tinker 2008 [9]
	$M \in [10^8, 10^{16}]M_\odot$	ΛCDM	Angulo [46]
	$\ln\sigma \in [-1.31, 0.55]$	ΛCDM	Watson [47]

Table 4: Details of the HMF fitting functions used in this paper. The various "nCDM" cold dark matter cosmologies are described in Table 3. For some fits, we have rewritten the function in terms of ν by substituting for σ and absorbing factors of δ_c into the original free parameters.

4 Data processing

This section summarises the N-body simulations and the process of extracting the halo catalogues which form our data. This includes our choice of halo finder, corrections and mass cuts to the binned halo counts and quantification of the uncertainties in the resulting discrete HMF.

4.1 N-body simulations

The N-body simulations were run using the `ISIS` and `ECOSMOG` code [48, 49], which is a modified gravity modification of the high-resolution N-body code `RAMSES` [50]. For details about the implementation and for a comparison of these codes see the modified gravity N-body code comparison project [51].

We ran two sets of simulations with different mass resolution. Simulation set 1 has $N = 512^3$ particles of mass $8.75 \times 10^9 M_\odot/h$ in a box of $B = 250$ Mpc$/h$. The background cosmology is a flat ΛCDM model with $\Omega_m = 0.269$, $\Omega_\Lambda = 0.732$, $h = 0.704$, $n_s = 0.966$ and $\sigma_8 = 0.8$. These simulations were presented in [51]. Simulation set 2 has $N = 256^3$ particles of mass $3.531 \times 10^{10} M_\odot/h$ in a box of $B = 200$ Mpc$/h$. The background cosmology is a flat ΛCDM model with $\Omega_m = 0.267$, $\Omega_\Lambda = 0.733$, $h = 0.719$, $n_s = 1.0$ and $\sigma_8 = 0.8$. These simulations were presented in [52].

Dark matter N-body simulations are performed by evolving two equations. The first one is the Poisson equation which gives us the gravitational potential Φ in terms of the particle positions (which determines the density field ρ_m)

$$\nabla_x^2 \Phi = 4\pi G(\rho_m - \overline{\rho}_m)a^2 \tag{4.1}$$

and the second is the geodesic equation

$$\ddot{\mathbf{x}} + 2H\dot{\mathbf{x}} = -\frac{\nabla_x \Phi}{a^2} \tag{4.2}$$

which determines the evolution of the particles. For the modified gravity simulations we consider here the only change is that we have a fifth force $-\nabla\varphi$ that contributes to the right hand side of Equation (4.2) and we have to solve a field equation similar to Equation (4.1), but highly non-linear, to get the fifth-force potential φ. More details about the implementation for the models considered in this paper are contained in [48, 51, 52].

We utilised two different halo finders of differing complexity:

1. The friend-of-friend halo-finder `MatchMaker`[7] with linking-length $b = 0.2$.
2. The 6D phase-space friend-of-friend halo-finder `RockStar` [53].

Both halo finders use the Friends-of-Friends (FoF) algorithm developed in [54], albeit with different distance measures. Particles are formed into connected graphs by drawing an edge between vertex particles if the distance between them is less than some fraction b of the mean inter-particle distance. Each connected graph is defined to be a halo if it is not a subgraph of a larger halo.

The `MatchMaker` finder is a parallel 3d-FoF finder. We used the canonical linking length $b = 0.2$. The distance between particles is the usual 3d Euclidean distance.

[7] MatchMaker can be found at https://github.com/damonge/MatchMaker

The `RockStar` finder uses the normal 3d FoF (albeit with $b = 0.28$) to identify groups of particles, within which it uses FoF in the 6d phase space to identify subgroups. After conversion from subgroups to subhaloes, any unbinding of particles from haloes is performed using the halo potentials. (This algorithm is summarised in Figure 1 of [53].)

Subsequently halo properties are extracted. The halo property with which we are concerned in this paper is the halo mass of the parent haloes only (i.e. we ignore subhaloes because we are only interested in the largest mass ranges). This is defined to be M_{200}, the total mass of all particles within the over-density satisfying $\rho \geq 200\rho_{\rm crit}$, where $\rho_{\rm crit}$ is the background critical density (not the matter density) [53].

A comparative analysis of halo finder performance in ΛCDM can be found in [55].

4.2 Simulation corrections

Having obtained our halo catalogues we now approximate the continuous HMF using a histogram.

We do not make any corrections to the data. Some authors propose adjusting the values of $\sigma(M)$ in the simulation data. The aim is to correct for the finite box size, which precludes modes with $k \leq 2\pi/L_{\rm box}$ from contributing to the over-density fluctuations in the halo. This effect can be approximated by the extended Press-Schechter approach (amongst other methods: see [11] for details). We avoid corrections for the mass variance due to our large box size, for which corrections are negligible.

It is necessary to remove simulation artifacts from the low-mass end. We truncate the mass function at a lower bound of 100 particles, where one particle is the mass resolution of the N-body simulations. (This is independent of the minimum number of particles required in the halo identification process.) Compared to the cuts of [11] this is a conservative cut: faced by a relatively small box size, we wish to retain as much of the HMF as possible. However, the cut is sufficient to remove the low-mass "tail" where the mass function—which should be monotonically-decreasing with mass—actually increases with mass. Such a phenomenon arises from the finite (mass) resolution of the simulations. At the lowest masses, there is insufficient resolution to identify all of the bound objects with few particles, so the number density is increasingly suppressed at masses below a characteristic turnover mass. This limitation cannot be alleviated without sub-sampling the simulation box at finer resolution. Slightly higher, at haloes with tens of particles, the uncertainty on the mass values is a significant fraction of the total halo mass. Consequently, the loss or addition of one particle can move the halo between bins. There are two possible ways of accounting for this: either incorporating a mass uncertainty in the likelihood function, or minimising the effect by judicious bin optimisation. We opt for the latter. This low-mass effect is well-known and we do not discuss it further.

At the high mass end our cutoff is artifically imposed by the finite box size. The finite box size curtails the number of large mass haloes found in a finite sub-volume of the horizon (this underestimation is quantified for ΛCDM in [8]). In addition, our excursion set technique prevents us from calculating the HMF for masses of $S < S_{\rm env}$ (for the excursion-set method) or $\nu_{\rm eff} < 0$ (for the cosmic web). Using a Gaussian window function with a radius of $10\,{\rm Mpc}/h$ this corresponds to a mass of $M \approx 10^{16} M_\odot$. We have confirmed that this does not remove any haloes from our data.

The remaining factor in our simulated HMF is the bin width of the histogram. The aim is to verify that the seemingly arbitrary bin choice (which varies in every HMF paper) has

minimal effect on the calibration of the free parameters. We adopted three constant-width bin methods, explained in the next paragraphs.

The constant bin width method is that most widely adopted in the literature. The haloes are typically binned in constant intervals of $\log_{10} M$ [39], or $\ln \sigma^{-1}$ [38], rather than $\ln \nu$, so the same $f(\nu)$ will produce a different (discrete) HMF in different MG theories. We adopt $\ln M$ to ensure a ready comparison between different gravity theories. A non-arbitrary method for selecting the bin width is to decide upon the maximum Poisson error tolerated and find the bin width ensuring this error in the most massive bin. (Lower-mass bins will have more haloes, hence less Poisson error.) However this produces an impractically small number of bins, of order the number of free parameters $(3-6)$ in the fitting functions. The advice of [13] is to leave the most massive bin variable and set a constant width for the other bins. While this method has the advantage of being directed by the simulation data, rather than arbitrarily selected, it produces relatively few bins. Instead, we applied $N = 10$ and $N = 100$ bins in order to approximate a choice of too few or too many bins. The former has difficulty accurately representing the steep gradient at the high-mass end, whereas the latter has such narrow bins that monotonic behaviour of the HMF is not observed, or even punctuated by zero-occupancy bins. This illustrates two possible dangers of arbitrarily selecting a number of bins.

In order for the bin width to be driven by the data, one can use Bayesian analysis to find an optimal number of bins. There exist a number of ways to find a "best" number of bins from a distribution by minimising the L_2 norm between the data and the underlying (unknown) smooth density function (e.g. [56]). However, it is possible to minimse the required assumptions using the method of [57], which computes the likelihood that the binned data is drawn from the smooth distribution. The bin width, i.e. amount of discretisation, which maximises this likelihood value is judged to be optimal. The downside of this method is the computational expense of the MCMC calculations required (to ensure that the uncertainty in the posterior mean is much less than half, i.e. we are certain to within a unit of one bin). However, for a one-dimensional histogram computed using ~ 50000 haloes, we found that this required ~ 1 minute per simulation. The results differ according to the gravity model used and the halo finder (as expected, for each has a different HMF). Since we did not wish to introduce another free parameter, we adopted a value of $N = 30$ bins as an average value across all our data sets.

4.3 Uncertainty in the data

Finally we quantify the uncertainty in the HMF.

The uncertainty in the bin occupation is assumed to be Poissonian. The usual uncertainty on bin occupations is taken to be the well-known result[8] that the Poisson standard deviation on a bin containing N haloes is $\sigma = \sqrt{N}$. Various HMF papers (e.g. [11]) use an "improved" Poisson error defined to be:

$$\sigma_{\pm} = \sqrt{N + \frac{1}{4}} \pm \frac{1}{2} \tag{4.3}$$

This asymmetric error asymptotes to the usual one for large N but is better-behaved for small N, particularly for empty bins. While this does not affect the Poisson-based likelihood, it

[8] Eq. (11) in [16] is not true, but is related to the standard deviation as a *fraction* of bin occupation: $\sigma/N = 1/\sqrt{N} \not\Rightarrow \sigma = 1/N$.

does enter the Gaussian-based likelihood. The reason is straightforward: the number of counts per bin is known precisely, so there is no uncertainty. The Poisson "noise" expresses the uncertainty in the mean of the underlying Poisson probability density function, which is equal to the variance term which does enter into the Gaussian probability density function. Since the error does not enter the likelihood function, we make no cuts when using constant-width bins (explained below). For variable-width bins, we tolerate an error of 10% or less, which is in line with the choice from other papers (e.g. [16]). We must pay attention to combining the asymmetric errors via the method of [58]. The combined variance is then:

$$V\left(x \,|\, \hat{x}\right) = V_0 + V_1(x - \hat{x}) \quad \text{where} \quad V_0 = \sigma_+\sigma_- \quad \text{and} \quad V_1 = \sigma_+ + \sigma_- \tag{4.4}$$

This method tightens the uncertainty on the low-occupation bins, weighting the Gaussian likelihood more favourably towards the high-mass end than with symmetric error bars.

5 Bayesian inference

The problems of both estimating the best-fit parameters in our fitting function and comparing between functions can be achieved simultaneously using Bayesian inference. First, we outline calculation of the posterior from the data using Bayes theorem. We define the likelihood functions used in this paper. We characterise different measures of the high-probability regions in our probability density functions for the HMF free parameters. The effects of the bin width, choice of likelihood function and nested sampling settings are discussed in Appendix B.

5.1 Priors

The priors I contain both our assumptions about the likelihood function and our prior distribution for the parameters of the hypothesis. We discuss the former in the next paragraph. The latter we set to uniform priors, i.e. we have no reason to favour any regions of parameter space over another. The lower limit for the priors is zero, because we must avoid an HMF which is negative (if the scaling parameter is $A < 0$), complex (fractional powers of $a\nu$ where $a < 0$), or non–monotonically-decreasing (since ν is an increasing function of mass, ν^p must have $p > 0$). The upper limit is arbitrary. Given that most published values for the parameters lie in $[0, 2]$ (the exception being Jenkins $a = 3.8$), we used an upper limit of 10 to ensure that the credible regions were well-contained within the prior region.

5.2 Choice of likelihood

Our aim is to find the posterior probability distribution $p\left(H \,|\, D, I\right)$ for a given hypothesis H when we take into account our prior information I and the data D. We have already examined D, the counts per mass bin from our simulation data in Section 4.2.

Now ew require an expression for the likelihood function $p\left(D \,|\, I, H\right)$. The choice of likelihood function largely reflects one's probabalistic education. The two schools of thought are typically a "Gaussian" likelihood based upon the frequentist chi-squared estimator and a "Poissonian" likelihood based upon maximum-entropy results from Bayes theorem. We choose between:

1. The Poisson likelihood (the last term is zero when n_i is zero):

$$\ln \mathcal{L} = -\sum_i \left(\mu_i - n_i + n_i \ln \frac{n_i}{\mu_i}\right) \tag{5.1}$$

2. The Gaussian likelihood with symmetric errors

$$\ln \mathcal{L} = -\frac{1}{2} \sum_i \left[2\pi V_0 + \frac{(\mu_i - n_i)^2}{V_0} \right] \tag{5.2}$$

3. The Gaussian likelihood with asymmetric errors

$$\ln \mathcal{L} = -\frac{1}{2} \sum_i \left[2\pi \left(V_0 + V_1(\mu_i - n_i) \right) + \frac{(\mu_i - n_i)^2}{V_0 + V_1(\mu_i - n_i)} \right] \tag{5.3}$$

where $\mu_i(\mathbf{q})$ is the number of counts (first-crossing distribution) given by the parameter set $\mathbf{q}$ and n_i is that given by the data in the i-th bin and the choice between counts and first-crossing distribution is determined by the use of the Poisson and Gaussian likelihood respectively. When applied to counts, n is always a positive integer, whereas μ is a positive real number. Bayesian inference implies that Equation (5.1) will produce the most accurate result, whereas the standard frequentist approach is equivalent to Equation (5.2). The last approach Equation (5.3) is no longer equivalent to the frequentist approach because the errors are asymmetric. We compare the results of Equation (5.1) and Equation (5.3) in Appendix B.

The likelihood $\mathcal{L}(H)$ is the probability that the hypothesis H produces the data D. However, we are interested in the probability that the data are consistent with the hypothesis. Via Bayes' theorem, we obtain:

$$p\left(H \,|\, D, I\right) = \frac{p\left(H \,|\, I\right) p\left(D \,|\, H, I\right)}{p\left(D \,|\, I\right)} \tag{5.4}$$

This is the complete posterior PDF for our hypothesis H in light of the data D given prior information I.

5.3 Parameter estimation

Having chosen a particular HMF, we are interested in the universality of the HMF across different MG theories. One way in which to measure this is to see how the best-fit parameter values change depending on the MG model. `MultiNest` gives three different options to define "best-fit": the maximum-likelihood (ML), maximum-a-posteriori (MAP) and posterior mean (PM) values.

The ML value for a given parameter θ is defined to be that which maximises $p\left(D \,|\, \theta, I\right)$, i.e. the most probable value for the model to give the observed data. In contrast the MAP value maximises the probability $p\left(\theta \,|\, D, I\right)$. Since we have chosen uniform priors, the MAP value is equal to the ML value via Equation (5.4). Since the ML value is the fastest to converge to the true value in MultiNest [59], we used this value for our best-fit parameters. We are also interested in the PM value

$$\langle \theta \rangle = \int \mathrm{d}\,\bar{\theta}\; p\left(\bar{\theta} \,|\, D, I\right) \bar{\theta} \tag{5.5}$$

because the 1σ credible regions given by MultiNest are only provided for the posterior mean.

If the full PDF is not well-described by a single value (e.g. the three values above are very different, or the posterior is very flat etc.), then we are better off examining the credible region R of credibility C, which is the set:

$$R = \left\{ \boldsymbol{\theta} : \int_{p\left(\bar{\boldsymbol{\theta}} \,|\, D, I\right) > c} d\bar{\boldsymbol{\theta}}\; p\left(\bar{\boldsymbol{\theta}} \,\middle|\, D, I\right) = C \right\} \tag{5.6}$$

where c is the level set forming the boundary ∂R, inside which the probability is greater than c and outside which it is less than c. We refer to the 1σ and 2σ credible regions for $C = 0.68$ and $C = 0.95$ respectively. This is particularly the case in multiple dimensions, e.g. examining correlations between variables. We show our results in Section 6.2 assuming the ΛCDM case for all our halo data and in Section 6.3 matching the excursion set model to the MG model for each dataset.

6 Results and discussion

This section addresses the questions posed in the introduction. Section 6.1 present our new results for incorporating MG into ΛCDM-calibrated HMFs. Appendix B confirms that our parameter estimation technique is reliable for the problem at hand. Then in Section 6.2 we discuss whether the presence of screened gravity can be mistaken for a change in best-fit parameter values for the ΛCDM HMF. In Section 6.3 we apply the procedure used in ΛCDM to calibrate the MG HMF using the full excursion set approach. We compare to existing values from the literature and assess the deviation. In particular we address the universality of the halo mass function, i.e. the invariance of the best fit free parameters to changes in the underlying gravity model.

6.1 Accounting for the drifting-and-diffusing barrier in MG

Section 6.1 presents our new results for incorporating MG into ΛCDM-calibrated HMFs.

In Section 3 we suggested a variety of different methods to implement the full effects of environment dependence in MG for a fitting function. We compare the data from our $f(\mathcal{R})$ simulations with $|f_{\mathcal{R}0}| = 10^{-5}$ and $|f_{\mathcal{R}0}| = 10^{-6}$ to the theoretical HMF using each method.

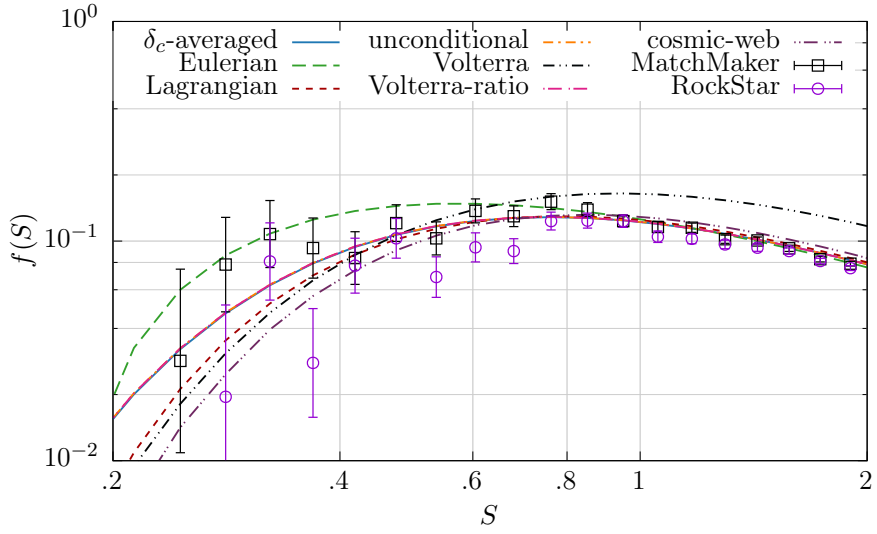

(a) ΛCDM

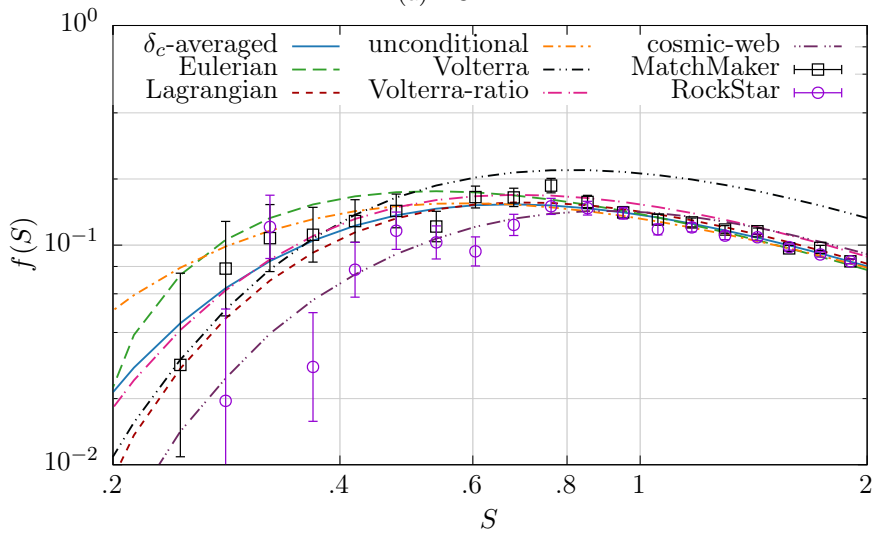

(b) $|f_{\mathcal{R}0}| = 10^{-5}$

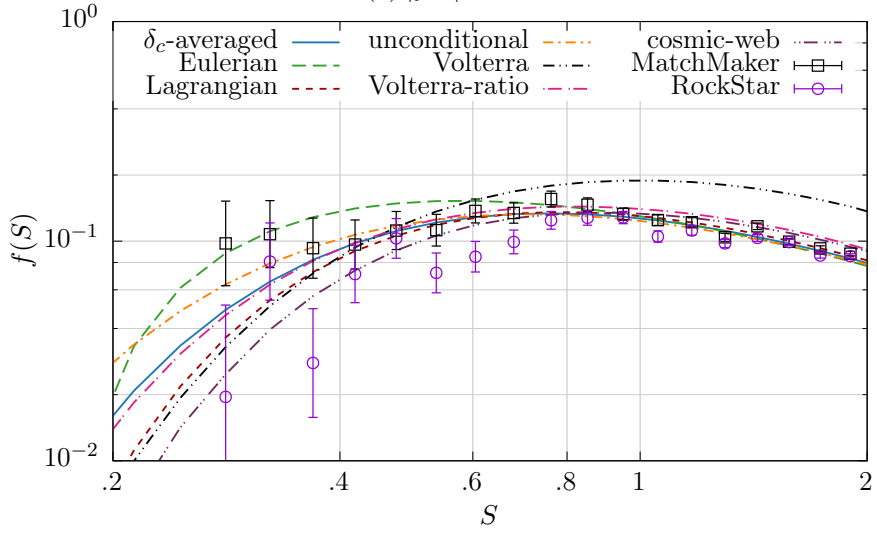

(c) $|f_{\mathcal{R}0}| = 10^{-6}$

Figure 4: The first-crossing distribution for a drifting-and-diffusing barrier using the variety of methods explored in this paper are shown as lines. We also plot the data from the N-body simulations using the two halo finders.

In the order given by Figure 4 we have:

1. The unconditional HMF using $\langle \delta_c \left(S \,|\, \delta_{\rm env}, S_{\rm env} \right) \rangle_{\rm env}$, the environment-averaged collapse density Equation (3.5)
2. The conditional HMF marginalised over the Eulerian $\delta_{\rm env}$-distribution Equation (3.7b)
3. The conditional HMF marginalised over the Lagrangian $\delta_{\rm env}$-distribution Equation (3.6)
4. The unconditional HMF, i.e. assuming both $\delta_{\rm env}$ and $S_{\rm env}$ vanish
5. The Volterra solution to Equation (3.1)
6. The unconditional HMF scaled with the Volterra solution using Equation (3.2)
7. The cosmic web HMF marginalised over the tidal tensor distribution Equation (3.4)

Figure 4 shows these methods for the Reed-07 fitting function[9] (lines) and the N-body HMFs calculated using the `MatchMaker` and `RockStar` halo finders (points). These simulations and the workings of the two halo finders are described in Section 4.1. We examine the ΛCDM results before discussing each method over the next few paragraphs.

The ΛCDM behaviour in Figure 4a is consistent with the excursion-set framework of [44]. The environment-averaged collapse density is δ_c^Λ (because the excursion-set barrier is flat) and the Volterra solution reduces to Press-Schechter. Therefore both of these methods produce the same result as the unconditional HMF. The other four methods all differ. While both the Lagrangian and cosmic web methods do equal the unconditional HMF using Press-Schechter, this is due specifically to the design of this function from excursion set theory. It is the only integrand for which the solution to the integral equation Equation (3.1a) is merely a rescaling between the conditional and unconditional forms of ν. We have now ensured that the different methods behave as expected in GR, before applying them to $f(\mathcal{R})$.

The first option avoids using excursion set theory altogether, by pre-emptively converting the drifting-and-diffusing barrier to an average density. The drifting barrier $\delta_c(S)$ can be incorporated straightforwardly, just as in the non-chameleon MG models, into the unconditional HMF. Surprisingly, this gives a very good fit, superior to the purely unconditional HMF. Although the peak of Equation (3.6) is at zero, this result illustrates that we need to use the entire PDF, rather than only using the peak to approximate the average. In this way we can account for the peak-background split, whereby it is easier for haloes to form as $\delta_{\rm env} \to \delta_c$ in dense regions and more difficult in under-dense regions. This method has the advantage that we can compute the barrier density once, rather than re-computing the conditional function at every stage of the MCMC process. We have managed to produce a good fit by considering only the barrier density, rather than accounting for the complex excursion set behaviour of the full drifting-and-diffusing barrier.

The conditional HMFs marginalised over the Lagrangian (Equation (3.6)) and Eulerian (Equation (3.7b)) theoretical distributions $p(\delta_{\rm env})$ have appeared in the literature before[10] [19], where they were applied to the Sheth-Tormen HMF. The authors suggested discarding

[9] We might have used any of the fitting functions, because our aim is to compare the behaviour of each technique for extending the mass function to MG. The Reed fit produced the closest fit to the data given the default parameters.

[10] [19] only plotted the relative enhancement $n_{\rm MG}(M) - n_{\rm GR}(M)/n_{\rm GR}(M)$, rather than the HMF proper $n(M)$, so we cannot readily compare our results to theirs.

the Lagrangian (density) distribution in favour of the Eulerian, on the basis that a density distribution which better reflects the physical formation of over-densities, would correspondingly produce a more accurate HMF. This is supported by the findings of [45]. While our results agree using the `MatchMaker` halo finder, the `RockStar` halo finder predicts a systematically lower distribution of haloes, better suited to the Lagrangian model. The question of which PDF to use is somewhat moot considering that neither fit performs particularly well. This is probably due to generating the conditional from the unconditional HMF. The rescaling at the end of ΛCDM excursion set theory which is used in [19, 34] implicitly assumes that a linear function of $\delta_c(S)$ is a good approximation for the actual barrier demsity. We have already seen in Figure 2 that this is not the case. Therefore we cannot use methods which work for a flat barrier density in ΛCDM to good effect in $f(\mathcal{R})$.

The solution to the integral equation is the MG-equivalent of Press-Schechter. For this reason, we do not expect it to be a good fit to the data. Indeed the $|f_{\mathcal{R}0}| = 10^{-5}$ anf $|f_{\mathcal{R}0}| = 10^{-6}$ plots in Figures 4b and 4c share the recognised flaws of the Press-Schechter fit in ΛCDM in Figure 4a, namely that it underpredicts at the high-mass end (low-S) and overpredicts at the low-mass end (high-S). Nonetheless, it reproduces the general behaviour of the first-crossing distribution, which is remarkable for such a simple model.

Moreover, we can improve the result from the unconditional HMF by scaling by the ratio of the Volterra solution to Press-Schechter. The two poor results combine to form a decent approximation. At the low-S end, the Volterra solution forms too few haloes becuase the random walks in excursion set theory are not absorbed early enough by the barrier density, so too many trajectories survive to produce haloes at high-S. In contrast, the unconditional HMF assumes $\delta_{\rm env} = 0$ (and $S_{\rm env} = 0$) so at small values of S the value of $\nu = \delta_c(S)/\sqrt{S}$ is large and vice-versa at high-S. Since the fitting function $f(\nu)$ is montonically increasing with ν, we have too many haloes at small S and too few at low S. These two behaviours counteract one another to reduce the overall discrepancy of the fit. This is because we have deliberately designed a method to combine different strengths of the analytical and empirical approaches. The unconditional fitting function is designed to produce a good approximation to the ΛCDM data. The Volterra solution captures the excursion set behaviour of the barrier density, which incorporates the main effect of $f(\mathcal{R})$ compared to ΛCDM from a theoretical viewpoint. Thus, we can combine two simple mechanisms to produce a relatively good solution, despite their individual predictions being ineffectual.

The performance of the cosmic web method is discussed in more detail in our previous paper [17]. In general it underpredicts the HMF at the high-mass end, whereas it works well at the low-mass end. There are two contributing factors, namely the $\nu_{\rm eff}$ approximation substituted into the fitting function and the $p(\rho, \theta, \nu_{\rm env})$ distribution related to the tidal tensor in the cosmic web. The former is not particularly successful even in ΛCDM ([60]) so we ought not expect any better performance in $f(\mathcal{R})$ where the spherical collapse in more complicated due to the fifth force. The latter is the equivalent of the Lagrangian distribution for $\delta_{\rm env}$ applied to all three eigenvalues of the tidal tensor rather than its trace. We have already seen that the Lagrangian-$\delta_{\rm env}$ fit does not produce an accurate fit. This technique is useful for calculating the HMF in individual structures of the cosmic web (e.g. voids, sheets etc.), wherein we have no other analytical treatment, but not the overall HMF.

Finally we comment on the distinction between the cosmic web results (Equation (3.4)) and those of the Lagrangian PDF. Given that the conditional HMF in the cosmic web doesn't depend upon (ρ, θ), and that the distributions for $p(\nu_{\rm env})$ and $p(\delta_{\rm env})$ have the same dependence on $\delta_{\rm env}$, one may expect that these two methods should produce the same results.

Clearly Figure 4 does not agree. This is due to the effect of the window functions in calculating $S(M)$ and $S_{\rm env}(R_{\rm env})$. In cosmic web we use a Gaussian window function for the environment and a (real-space) top-hat for the halo, whereas in the excursion set we used a top-hat window function for both halo and environment. This affects the value of $S_{\rm env}$ obtained from the same environment radius. Additionally, the Lagrangian (and Eulerian) result(s) both assume that the halo-environment correlation is $\epsilon = S_{\rm env}/S$. This is due to the assumption in excursion set theory that our trajectories in (δ, S) are uncorrelated at successive values of S, for which one requires a sharp-k window function, whence comes this expression for ϵ. In the cosmic web method we calculate ϵ numerically for a Gaussian and top-hat window function in the environment and halo respectively. Therefore the same values of $\delta_c(S|\delta_{\rm env}, S_{\rm env})$ map differently onto the argument of the conditional HMF. Once this is established, it does not matter that the marginalisation over the environment is the same in both methods.

Given the performance of the various technique for extending the fitting functions to chameleon MG, and the performance factor involved in re-calculating a conditional HMF (and marginalising over it) at every stage of the MCMC procedure, we shall use the Volterra-ratio method to calculate the $f(\mathcal{R})$ HMF in Section 6.3. Nevertheless, we have found a broad spectrum of possible methods by means of which we can incorporate MG into fitting functions originally designed for ΛCDM alone. Moreover, we have found that some are more suited to certain applications (e.g. the cosmic web approach) or halo finders (e.g. the two density-marginalised methods) than others. This demonstrates the additional complexity which environment dependence produces in chameleon screening compared to symmetron- and Vainshtein-screened theories. We cannot neglect this and simply substitute the unconditional HMF if we wish to produce a useful empirical function to use in lieu of deriving one from N-body simulations.

6.2 Assuming concordance cosmology

The first problem is perhaps so obvious as to be invisible: if we do not set out to look for modified gravity, we may be unable to detect it. In other words, having assumed a ΛCDM cosmology *a priori*, does modified gravity present itself *a posteriori* as merely a different (i.e., non-standard) set of best-fit parameters in a ΛCDM halo mass function? In this subsection, we fit the N-body HMFs for each modified gravity model using the ΛCDM mass functions. We used 10^2 and 10^3 live points to ensure that our results had converged, i.e. that our estimate of the posteriors PDFs was accurate. We also examined the effects of both the `MatchMaker` and `RockStar` halo finders, which we expect to differ due to their varying criteria for finding bound objects, which translates into a different halo mass function.

First we define appropriate criteria for a fitting function to produce a well-behaved fit to the data. We define a fit to be "successful" if the credible regions are continuous, smooth and peaked, tending to zero well within the prior parameter range. We do not exclude a fit form being well-behaved if zero is within its 1σ credible region: instead we examine the proximity of the maximum-a-posteriori value, excluding the fit if the probability at zero is close to that of the MAP. (A more quantitative option would be to exclude a fit if zero lies within the full-width-half-maximum of the Gaussian posterior, but we cannot guarantee that our posteriors are Gaussian.) The upper limit is set by the priors, so our main criterion is the breadth of the posterior. If it does not have a clear peak (or peaks), but a flat posterior, then there is too much uncertainty for the fit to be useful: it is not constrained by the data.

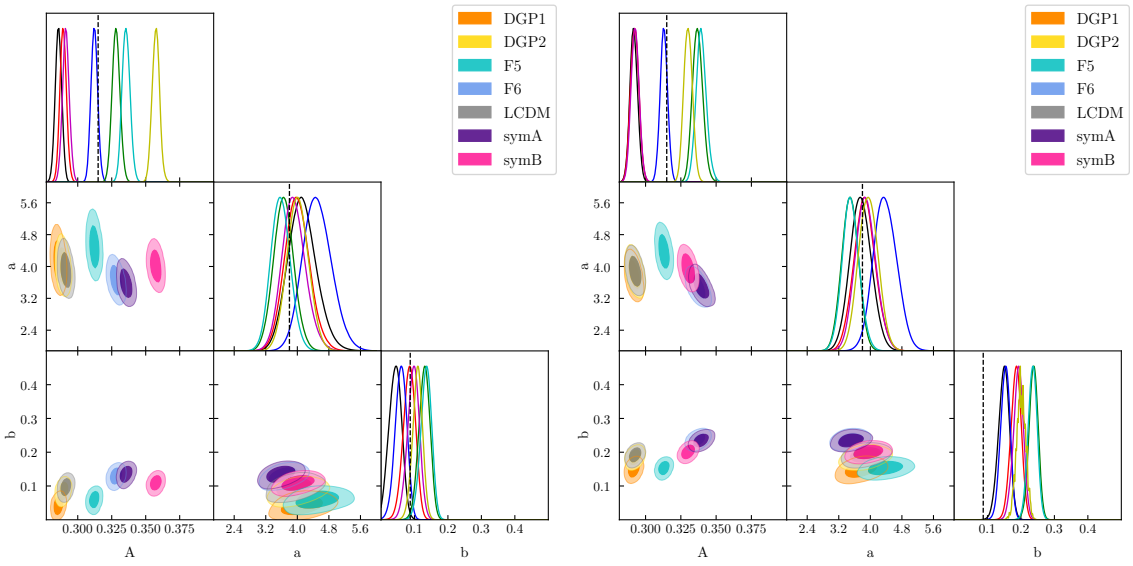

(a) ΛCDM: MatchMaker halofinder, 30 bins

(b) ΛCDM: RockStar halofinder, 30 bins

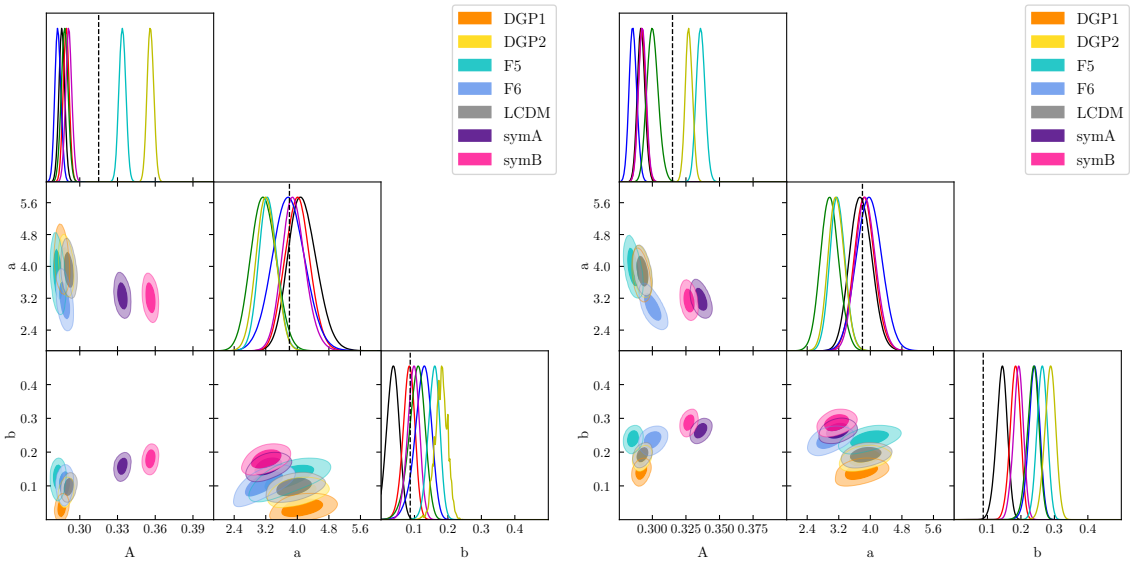

(c) MG: MatchMaker halofinder, 30 bins

(d) MG: RockStar halofinder, 30 bins

Figure 5: Posteriors for the Jenkins HMF calculated for each gravity model. The main diagonal shows the 1-d posteriors marginalised over all other parameters, while the off-diagonal plots show correlations between pairs of parameters via the 2-d $1, 2\sigma$ credible regions. The black dashed lines show the values proposed by [38].

The majority of the mass functions are well-behaved for all MG models and both halo finders: Peacock (Figure 6), Jenkins (Figure 5). Initially, SMT-Courtin (Figure 7) appears to not be succesful because both halo finders and all MG models have a peak as p approaches zero. However, this lower bound is set by the physical requirement for the parameters to be

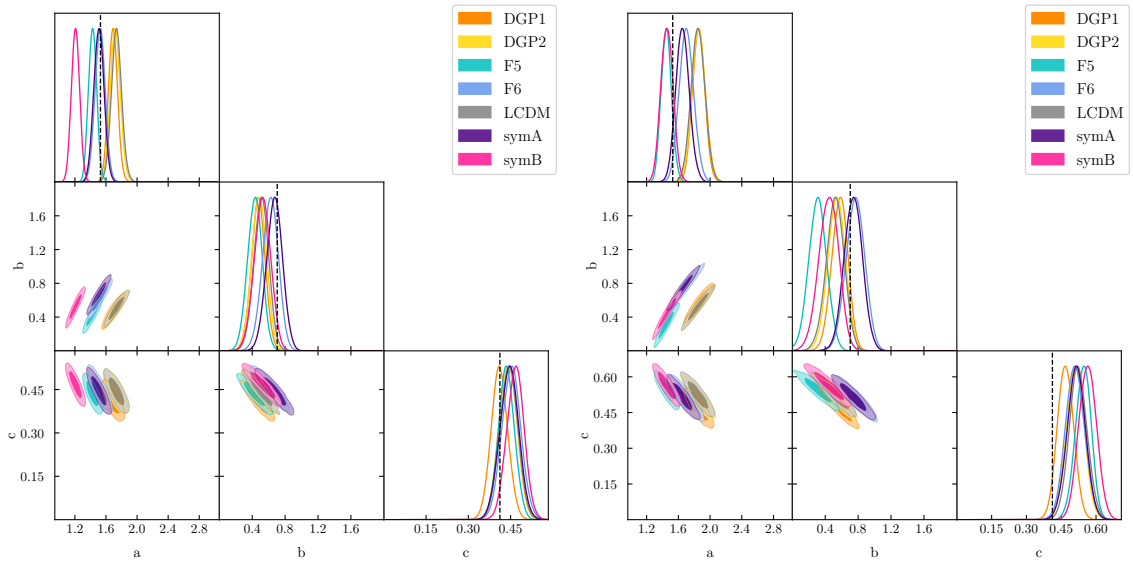

(a) ΛCDM: MatchMaker halofinder, 30 bins

(b) ΛCDM: RockStar halofinder, 30 bins

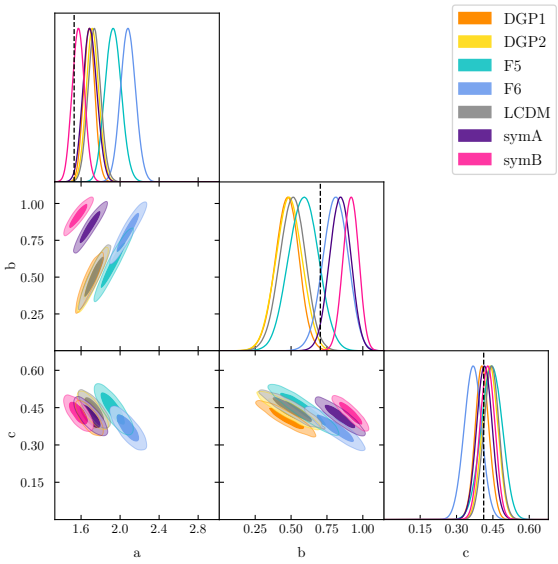

(c) MG: MatchMaker halofinder, 30 bins

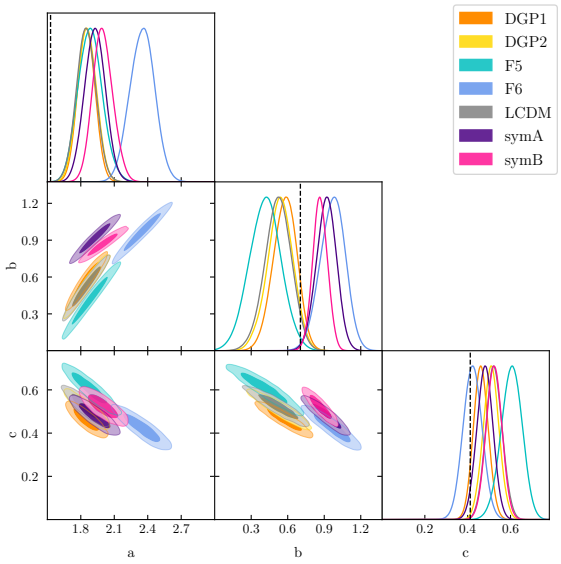

(d) MG: RockStar halofinder, 30 bins

Figure 6: Posteriors for the Peacock HMF for each gravity model. The main diagonal shows the 1-d posteriors marginalised over all other parameters, while the off-diagonal plots show correlations between pairs of parameters via the 2-d $1, 2\sigma$ credible regions. The black dashed lines show the values proposed by [40].

positive, rather than an indication that we have not explored enough of the parameter space. Moreover, considering that the prior volume of p is in $[0, 10]$, the motion of the maximum-likelihood from 0.1 (Courtin et al.'s original value) to 0.0 is only a 1% shift relative to the size of the parameter space. The Warren-Crocce fitting function exhibits slightly different

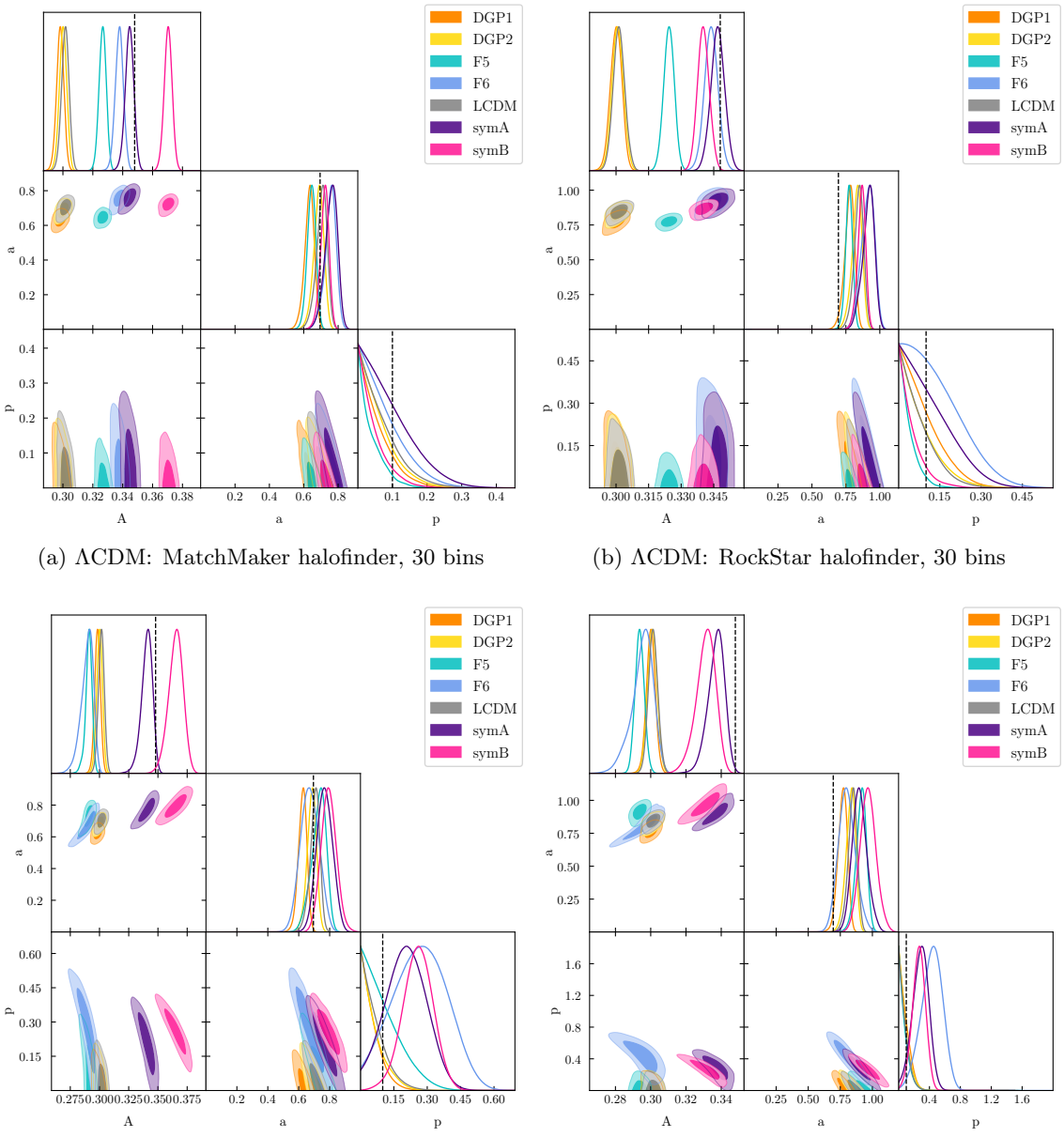

(a) ΛCDM: MatchMaker halofinder, 30 bins

(b) ΛCDM: RockStar halofinder, 30 bins

(c) MG: MatchMaker halofinder, 100 bins

(d) MG: RockStar halofinder, 100 bins

Figure 7: Posteriors for the SMT-Courtin HMF for each gravity model. The main diagonal shows the 1-d posteriors marginalised over all other parameters, while the off-diagonal plots show correlations between pairs of parameters via the 2-d $1, 2\sigma$ credible regions. The black dashed lines show the values proposed by [16].

behaviour in Figure 8 for b. Using the `MatchMaker` finder, only LCDM, DGP1 and F5 peak clearly away from $b \approx 0$; whereas using `RockStar` only SymB peaks at $b \approx 0$. The same logic applies as with SMT-Courtin, except that we can be more reassured here because the majority of MG models produce a ML value at the published value (the black dashed line).

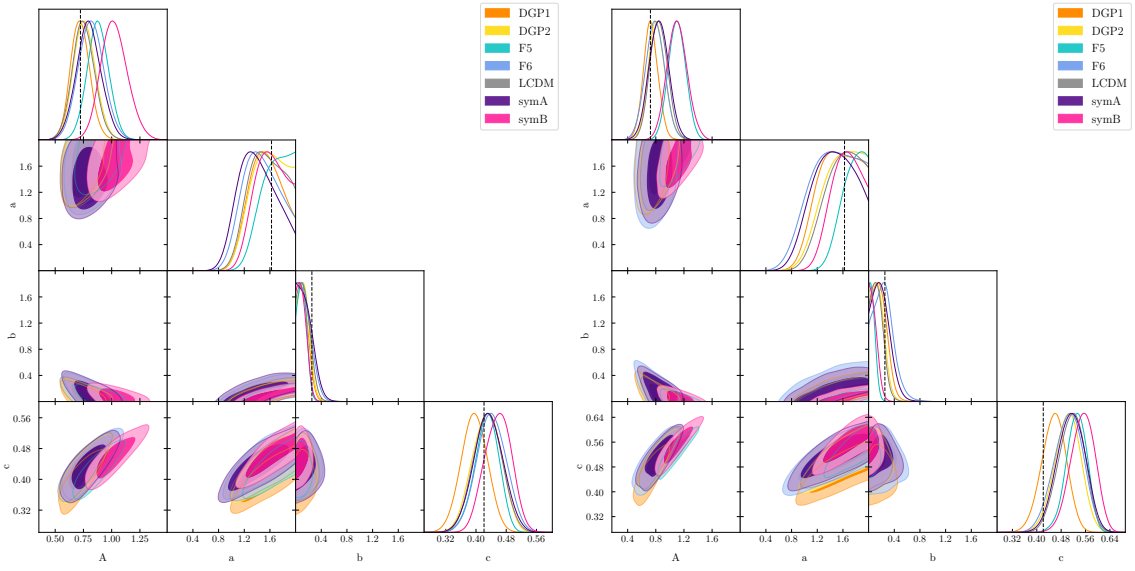

(a) ΛCDM: MatchMaker halofinder, 30 bins

(b) ΛCDM: RockStar halofinder, 30 bins

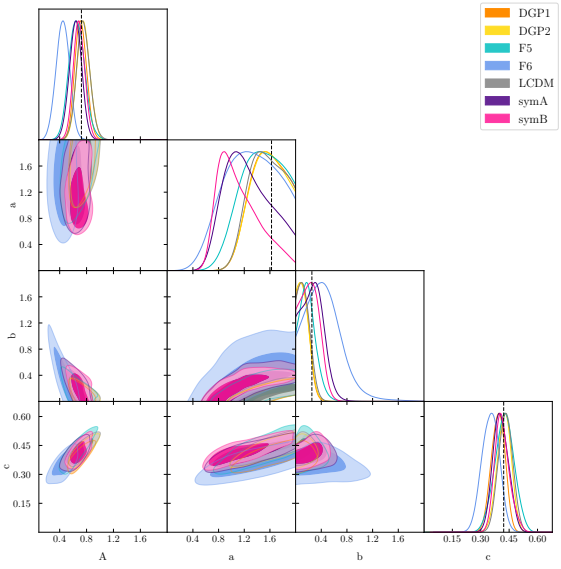

(c) MG: MatchMaker halofinder, 30 bins

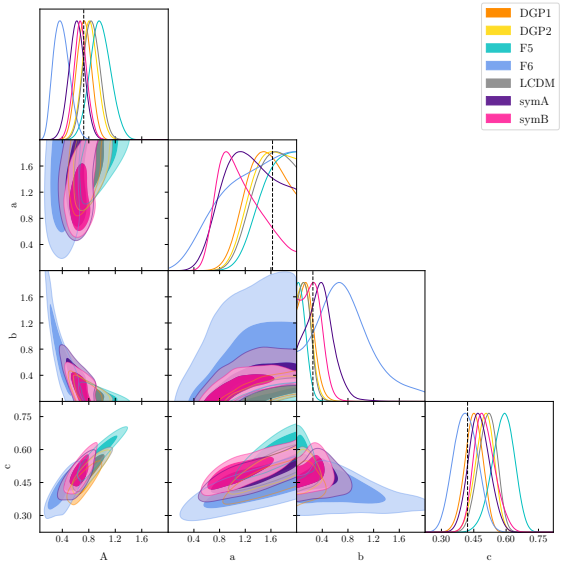

(d) MG: RockStar halofinder, 30 bins

Figure 8: Posteriors for the Warren-Crocce HMF for each gravity model. The main diagonal shows the 1-d posteriors marginalised over all other parameters, while the off-diagonal plots show correlations between pairs of parameters via the 2-d $1, 2\sigma$ credible regions. The black dashed lines show the values proposed by [13].

However, the posteriors are broader and more complicated in shape than the simple peaks for the other HMFs. This is probably due to the corrections made to the mass of each halo when Warren et al. derived the function: a halo of N particles was corrected to $N(1-N^{-0.6})$, producing a non-linear correction to the resulting $n(M)$. In this way we have found that all

of our fitting functions can exhibit a degeneracy between a change in cosmology and a change in the underlying gravity theory.

We can now determine whether some HMFs are more sensitive to the underlying theory of gravity than others. A halo mass function whose parameters have credible regions highly insensitive to the gravity model which generated the N-body halo data is one in which we are unlikely to detect deviations from general relativity inadvertently. Conversely, should the values of (or degeneracies between) parameters change sufficiently between N-body simulation "data", then we have an HMF in which deviations from ΛCDM values may reliably indicate the underlying deviation from an ΛCDM cosmology. Our results lie somewhere between these extremes: we can use a subset of the free parameters to distinguish between different classes of models, but cannot really test the parameters in the MG models themselves.

For example, Jenkins shows a high degree of overlap between all the MG models for a and b, so we must rely on A. Certain MG theories are clearly distinct (F5, SymA and SymB) whereas DGP and LCDM are nearly indistinguishable and F6 has some overlap with the two symmetron models. Thus we can clearly identify whether a result is in one of the DGP-LCDM or Sym-FR "families" but not confidently be more specific.

Similarly, the Peacock model is nearly indistinguishable for b and c, despite showing a spread of best-fit values for the remaining parameter A. This spread differs depending upon the halo finder: for `RockStar` there is some overlap between the three "families", whereas for `MatchMaker` the families are more distinct.

The situation is even more problematic for the SMT-Courtin fit, where not only does a have significant overlap, but p peaks to the same value for all MG models. Once again for A we may reasonably expect to separate the DGP and LCDM models (themselves inseparable) from the F5 model, and this from the F6 and Symmetron ones.

The Warren-Crocce model with `MatchMaker` has only three well-behaved MG results, so we can use A to readily distinguish between DGP1, F5 and SymB. Conversely, the `RockStar` result has too much overlap to determine the underlying MG model.

Therefore we find that is it possible for MG to be mis-interpreted as a ΛCDM result for most of the fitting functions, bar Tinker-Angulo-Watson. However, we cannot distinguish between the underlying mechanisms for the deviation from ΛCDM. The same trends occur: the separation of LCDM and the two DGP models into one group and the $f(\mathcal{R})$ and Symmetron ones into one or more others.

However, we cannot readily use this to test for varying theories of MG because the fitting functions display considerable similarities in their credible regions, so we are forced to rely on one or two parameters where the variation is distinctive. Nonetheless, it is remarkable that MG theories which have not only additional fifth-force interaction governing their spherical collapse, but also more complex excursion set behaviour, can be well-approximated by the HMF functions derived from ΛCDM simulations. Consequently, we do not necessarily have to reproduce the approach used in GR, i.e. inventing new functions and calibrating them.

6.3 Recalibrating best-fit parameters

Now we explore the opposite question to the previous one, namely: how universal is the halo mass function? In this subsection, we use the same extended gravity model for both the N-body data and the collapse density for the halo mass function. In this way, insensitivity of the credible regions for the fitting function parameters to the gravity model used would indicate that the halo mass function in question is "universal" in a greater sense than that which is currently applied. Not only would it be insensitive to the redshift, but also to the model

of gravitational collapse under which the haloes formed. This would vindicate the current practice to derive and calibrate HMF functions in ΛCDM N-body simulations alone—with the advantage that they could then be reliably applied to any scalar theory of MG with the same cosmological parameters.

Figures 5 to 8 show the 1,2-σ credible regions for the free parameters in each of the fitting functions which passed our tests in Appendix B. As in the previous subsection, the main diagonal show the 1-d posteriors marginalised over all other parameters, while the off-diagonal plots show correlations between pairs of parameters via the 2-d credible regions at $1, 2$-σ. The black dashed lines show the published values for each HMF, i.e. those proposed by their original authors. (Where it is not visible, the value is outside the range of the plot provided by `GetDist`.) We examined the behaviour of both the `MatchMaker` and `RockStar` halo finders.

Should we expect the LCDM results from our calculations to equal those from the original values of their respective papers? We do not expect to recover these results for a variety of reasons:

- The value of δ_c changes with Ω_{m0} and H_0
- The value of σ depends upon the power spectrum and value of σ_8
- Differing halo finders and settings
- The presence (or absence) of corrections to the N-body halo data

Let us examine each of these in turn.

Table 3 summarises the cosmological parameters used for each of the papers which provided "best-fit" parameters for particular fitting functions. The dependence of δ_c^Λ on Ω_{m0} is given in parametric form by [61] as $\delta_c = 1.68/\Omega_{m0}^{0.28}$. Our value is $\delta_c^\Lambda \approx 1.675$. This contrasts with most of the papers (bar [16]). Some [36, 40, 41] use the SCDM value $\delta_c \approx 1.686$ (following Press-Schechter [7]) regardless of the actual cosmology of their simulations. Others [9, 13, 38, 46, 47] absorb the value of δ_c into their free parameters because they use σ as the independent variable rather than ν, so their choice—which we need to convert back to ν—is ambiguous. In all cases we have assumed the exact SCDM collapse value $\delta_c = 3 \cdot (12\pi)^{2/3}/20$ when converting from σ to ν. Only [16] vary δ_c according to the solution of the spherical collapse equation for a variety of cosmologies. Thus we have a different numerator for ν. Moreover, it is unlikely that our $P(k)$ is precisely equal to any of those used in the papers.

Even if it did match, the normalisation σ_8 differs. The variance σ which forms the denominator of ν therefore also differs from previous publications. Since the independent variable ν (or more precisely, our mapping $\ln M \to \nu$ from counts to first-crossing distribution) differs in this paper (and indeed in all of the others), our free parameters must change to compensate. Even if we had exactly the same numbers of counts and the same bins, and our best-fit HMF had the same $n(M)$ values as a preceding paper, we would see a change in $f(\nu)$. This is a small contribution to the movement of the maximum-likelihood peaks from the published values.

The choice of halo finder further abstracts the problem. All of the published values except Peacock and Watson (both of which are FoF-only) arise from a compromise between the best-fit values for multiple halo finders. For example, Jenkins [38] uses both FoF and SO halo finders to find a fitting function which has a residual of within 20% compared to their N-body HMFs simulated for a range of cosmologies (not just ΛCDM). Even when restricting

their data to FoF-only and SO-only (whereby they obtain different best-fit values), the FoF linking length is changed between cosmologies ($b = 0.2$ for τCDM, $b = 0.164$ for ΛCDM), so we cannot disentangle the cosmological effects from the reduction of the N-body "data". As we can see by comparing the results for `MatchMaker` and `RockStar` in Figures 5 to 8, the same distribution of mass within the N-body simulations produces a different HMF according to the halo finder used. [55] discuss this in great detail for ΛCDM and we have no reason to disagree with their findings.

Differing authors also treat the distribution $n(M)$ obtained from their halo finder(s) in a variety of ways. As we briefly covered in Section 4, the mass cutoffs are controlled by the simulation box size and the mass resolution. Table 4 summarises the mass range used by each paper. This shifts the sampling along a subsection of the actual HMF, changing the influence of each parameter in the likelihood function. An extreme example of this is the Reed 2003 fit, whose parameter c is completely unconstrained by masses $M \leq 10^{15} M_{\odot}$ [14]. Sometimes the individual halo masses are systematically "corrected", e.g. [2] or (more relevantly here) the Warren correction: a halo of N particles was updated to $N(1 - N^{-0.6})$ to account for perceived flaws in the halo finders. These factors all affect the final first-crossing distribution of the data, against which is compared the first-crossing distribution of the model (converted to counts per bin) which contains the values of the free parameters at a chosen point in the parameter volume.

Given these factors, it is not surprising that our LCDM values do not always align with the published values. In Figures 5 to 8 the grey lines show our ΛCDM posteriors, while the black dashed lines show the values from one of the relevant papers respectively. (We do not show all of the published values for every fitting function because this would lead to up to five lines on some plots, which would be confusing.) Of particular interest is the variety of best-fit values for the SMT fitting function. Our changes in all HMFs are the same order of magnitude as the changes other authors have found when altering the cosmological parameters, halo finders and data reduction techniques used to derive the HMF. Since we are utilising a single cosmology and separating the effects of our two halo finders, it is not surprising that our values do not reproduce the existing ones.

Despite the fact that we have used the full MG modifications to $\nu\left(S \,|\, \delta_{\rm env}, S_{\rm env}\right)$, the behaviour of the HMFs mirrors that of the previous subsection, in which we assumed $\nu = \delta_c^{\Lambda}/S$. Some HMFs have precisely the same "good behaviour" (or lack thereof) in both cases. The Jenkins plot has the same flaws with $b \approx 0$ for DGP1 in Figure 5c (cf. Figure 5c). The Peacock plot has the same multi-modal tendencies for c in Figure 6c and Figure 6c. Otherwise these HMFs have well-behaved posteriors. SMT-Courtin in Figure 7 is well-behaved for all MG theories and both halo finders.

It is notable that the Peacock HMF—an empirically-derived fit to the Watson-FoF HMF accurate to 1% in ΛCDM—does behave well when generalised, whereas the original Watson fit does not. This suggests that the behaviour is not caused by over-simplifying the gravitational collapse, but by the underlying form of the fitting function itself. In contrast, Warren-Crocce shows considerable improvement in terms of the poor behaviour of the posteriors peaking at $b \approx 0$ in both Figure 8 and Figure 8. However for the `MatchMaker` result, both F5,6 models are well-behaved in MG, compared to F5 alone in ΛCDM; moreover `RockStar` behaves (relatively) well for everything apart from SymB. In this case, accounting for the mass dependence of the critical density does improve the behaviour of the HMF. Thus we see that generalising ν from its ΛCDM value (proportional to σ^{-1}) to MG does not affect the overall behaviour of the HMFs, compared to the previous subsection.

We can use the HMFs to examine the universality of ν: specifically, whether accounting for the excursion set behaviour of the MG models is sufficient to render our fitting functions independent of MG. While it is evident from Figures 5 to 7 that no single value works for every MG model, we do find clustering between families. The Jenkins posteriors (Figure 5) show that the credible regions for the two symmetron models are quite distinct from the other five models, all of which have overlapping credible regions. The Peacock function shows a higher degree of universality than Jenkins: particularly in Figure 6c, but slightly less in Figure 6d. In particular c is practically universal, but there is a spread of overlapping values for the other two parameters. SMT-Courtin (Figure 7) has very similar behaviour to the Jenkins HMF, with the two Symmetron models distinct from each other as well as the clustering–but here it is four of the other five models, with F6 closer to the Symmetron results. Unlike the preceding fitting functions, Warren-Crocce (Figure 8) has posteriors which largely overlap, perhaps with the exception of F6, and more clustering in `MatchMaker` than `RockStar`. This fitting function has no credible regions which are isolated from one other. Thus, the fitting functions display a range of behaviours, but most show that the best-fit parameter values for multiple MG models do overlap.

Where the symmetron models are distinguishable from the others, the differences are driven by the "normalisation[11] factor:" the symmetron models underpredict $n(M)$, requiring a systematic upwards shift by increasing the multiplicative factor A. These models have a drifting barrier $\delta_c(S)$ which includes mass dependence. However, this dependence via the collapse density ODE is not accounting for all of the actual behaviour of the haloes in non-linear collapse. Considering that we use a simple model of a collapsing spherical top-hat, we may be oversimplifying the effect of the symmetron fifth-force.

There is also the issue of the F5 and F6 models exhibiting greater spread (albeit still with overlapping credible regions) than the LCDM and DGP results. This is particularly visible in Warren-Crocce. Recall that here we fully account for the excursion-set barrier density using the Volterra solution. However, we use this to scale the unconditional HMF, so we approximate the integral over the environmental dependence of the HMF via the value at the peak of the environment distribution (which happens to be $\delta_{\rm env} = 0$). Under these circumstances, it is remarkable that our approximation does produce such a universal result.

The two DGP models cluster strongly with ΛCDM in all the HMFs. This is possibly because all of these models use a flat barrier, so there is no additional mass- or environment-dependence to be included in ν, so no additional excursion set behaviour which needs to be approximated by the change in the independent variable.

While we do not find a strong degree of overall universality, we can see that the different screening mechanisms do behave similarly. This is independent of the choice of halo finder, so this clustering is not caused by systematic effects or scatter in the N-body data.

This illustrates the caution which must be employed when using fitting function originally calibrated in ΛCDM in the context of MG. Although the generalisation of the fitting functions from ΛCDM to MG does not produce a completely universal fitting function, there is a degree of universality in the clustering of the credible regions for different screening mechanisms. This is because the effects of the fifth-force are largely encapsulated by the modified Poisson equation which appears in the ODE for gravitational collapse. The resulting δ_c clearly does not contain all of the non-linear collapse information (otherwise we *would* have

[11] While A originally played this role in the SMT-Courtin function [36], we no longer require the cumulative mass fraction to tend to unity.

a universal HMF) but it does incorporate enough into ν that the resulting fitting function depends only on the type of screening, rather than the values of the fifth-force parameters.

7 Conclusions

This section reiterates the salient points of this paper. We outline the method we have used, before describing avenues for generalisation and other possibilities for further work. We conclude by summarising the key results of this paper.

7.1 Summary

In this paper, we explored the use of the halo mass function in screened MG theories. We selected a range of theories which have different screening mechanisms (Appendices A.1 to A.3) and derived their additional contribution to the Poisson equation. We summarised a variety of HMFs and described the nature of their universality in GR and how to transform this into the equivalent in MG (Section 3). The N-body simulations from which we extracted halo catalogues to compare to our empirical fits are described in Section 4.1. Similarly, the Bayesian methodology for estimating maximum-likelihood parameters and the relative likelihood of the different models is outlined in Section 5. The key steps of our method are:

1. Conversion of the GR HMF from σ to ν (if necessary).
2. Calculation of the effective fifth-force $F_{\rm eff}$ to insert into the spherical collapse ODE.
3. Calculations of the collapse density $\delta_c(S, \delta_{\rm env}, Senv)$ to incorporate into ν.
4. Use of an appropriate excursion-set technique to account for the barrier density δ_c.
5. MCMC estimation of the best-fit free parameter values and their credible regions.
6. Output of the corresponding best-fit HMF.

Our main results (Section 6) are as follows.

We found a broad spectrum of possible methods—some newly-proposed in this paper—by means of which we can incorporate MG into fitting functions originally designed for ΛCDM alone. Of the various techniques for extending the fitting functions to chameleon MG, we have found that some are more suited to certain applications (e.g. the cosmic web approach) or halo finders (e.g. the two density-marginalised methods) than others. This demonstrates the additional complexity which environment dependence produces in chameleon screening compared to symmetron- and Vainshtein-screened theories. We cannot neglect this and simply substitute the unconditional HMF if we wish to produce a useful empirical function to use in lieu of deriving one from N-body simulations.

We found that the effects of MG can be interpreted as a change in best-fit parameters in the ΛCDM HMF for all of the fitting functions. Alternatively, the relation can be inverted to judge the universality of the HMF, i.e. its independence on the underlying theory of gravity. Although we found no completely universal HMF, the parameter values did cluster according to the type of screening mechanism, with Jenkins, Peacock and SMT-Courtin being the least universal and Warren-Crocce the most. The former group required very different best-fit parameters for the two Symmetron models, whereas in the latter all of the models had overlapping credible regions. The results suggest that a single, best-fit HMF might be

used for each type of screening, independent of the parameters in the MG model. This demonstrates that the additional complexity of the gravitational collapse in screened MG theories cannot always be accounted for using the techniques developed in GR. However, it is unnecessary to develop new fitting functions and calibrate them on a case-by-case basis.

We have demonstrated that it is possible to generalise some of the halo mass functions in common use in GR to incorporate MG theories with a variety of screening mechanisms. However, the calibration of these fitting functions has a number of caveats which are not encountered in the ΛCDM framework for which they were initially developed. Nonetheless, it is remarkable that our method can incorporate much of the non-linear collapse behaviour of screened MG in a simple and efficient mechanism. This is in direct contrast to the difficulties encountered in performing N-body simulations in screened MG. Thus we have provided an excursion-set-motivated alternative in MG to the need to replicate the time-consuming development of accurate halo mass functions which took place (and is ongoing) in GR.

7.2 Further work

The method presented in this paper for calculation of the MG halo mass function using the fitting functions derived from ΛCDM has many avenues for generalisation. Most straightforward of these is the application to other fitting functions as they become available, provided that these functions can be expressed in terms of the "universal parameter" ν rather than the variance σ.

The universality of the halo mass function can be further extended to higher redshifts. The collapse ODE (derived in [34]) has a new stopping condition that $y_h(z_c) = 0$, but the same bijection scheme can be applied to calculate the collapse density $\delta_c(z_c)$. The variance $\sigma(z)$ is obtained from the present-day value via the growth factor $D(z)$. However, to a good approximation, these modifications cancel, leaving ν independent of z [1]. This generalisation is particularly relevant given the ongoing discussion on the z-independence of $f(\nu)$ in ΛCDM. It would be particularly interesting to determine the influence of the fifth-force on the evolution of the HMF.

The calibration techniques are applicable to any MG theory which satisfies the following:

- Existence of a modified Poisson equation to approximate the modifications to gravity
- Well-posedness of the corresponding spherical-collapse ODE
- Background expansion similar to ΛCDM (so that the ΛCDM growth factor can be used and the halo environment treated as ΛCDM in the collapse ODE)

Galileon MG is an example of a screened theory for which this technique may be used. However, it may also be applied to MG theories which do not involve screening, but have some other method of being observationally-viable. It would be interesting to investigate whether the results we have found are unique to screening models, or whether they extend to non-screened theories.

The cosmology-dependence of these results can also be explored. This would be a daunting task, requiring N-body simulations for a grid of cosmological parameters, especially given the additional complexity of incorporating a fifth-force into the simulations. Nonetheless, this would permit comparison with the investigation of the cosmological-dependence of the HMF in GR (e.g. [16]). Moreover, if using changes in the best-fit GR parameters for a given fitting

function to suggest a deviation from ΛCDM, it would highlight the potential degeneracy between a change in MG and a change in the GR cosmological parameters. This is important if we are to use the HMF as a probe of MG in future surveys.

The many avenues for generalisation illustrate that the same attention to detail can be applied to the HMF in both ΛCDM and MG. Having illustrated a number of caveats—the choice of fitting function, likelihood and the dependence of the results on both halo finder and bin width—we nonetheless show that three common HMFs can be used and calibrated in both GR and MG. Without applying the same calibration techniques in both theories, we are not making a like-for-like comparison when analysing the behaviour of the HMF, especially when constructing theoretical HMFs to compare to observations.

Acknowledgements

We would like to thank Hans Winther for useful feedback on the many drafts and Pedro Ferreira for useful comments and discussions.

A Screened gravity theories

A.1 $f(\mathcal{R})$ gravity

An $f(\mathcal{R})$ theory can be defined in the Jordan frame via the action:

$$S_J = \int d^4x\sqrt{-g}\,\frac{1}{2}\left[\mathcal{R} + f(\mathcal{R})\right] + \mathcal{L}_{\rm m}\left[\Phi_i, g_{\mu\nu}\right] \tag{A.1}$$

where we have (temporarily) chosen units such that $8\pi G = 1$, the function $f(\mathcal{R})$ is a general function of the Ricci scalar $\mathcal{R}$ and Φ_i denotes all matter fields.

The $f(\mathcal{R})$ modification in the Jordan frame translates to a scalar-tensor theory of gravity in the Einstein frame where the scalar field ϕ is coupled to matter. The fact that we have this conformal transformation is the essential ingredient behind the mapping between $f(\mathcal{R})$ and chameleon-screened theories [62].

The explicit $f(\mathcal{R})$ model which we apply here is the Hu-Sawicki model of [30]. This is a well studied model known to exhibit chameleon screening [63]. The value of $|f_{\mathcal{R}0}|$, the value of $f(\mathcal{R})$ in the cosmological background evaluated at $z = 0$:

$$|f_{\mathcal{R}0}| = n_{f(\mathcal{R})}\frac{|c_1|}{c_2^2}\left(\frac{\Omega_m}{3(\Omega_m + 4\Omega_\Lambda)}\right)^{1+n_{f(\mathcal{R})}} \tag{A.2}$$

determines the magnitude of variations from ΛCDM. Throughout this paper we set $n_{f(\mathcal{R})} = 1$ and will only consider $|f_{\mathcal{R}0}| = 10^{-5}$ and $|f_{\mathcal{R}0}| = 10^{-6}$.

To see how screening works, let us consider a top-hat over-density of radius $R_{\rm TH}$ and mass $M_{\rm TH}$. As shown in [64] the enhancement of the gravitational force on a test-mass of mass m outside the top-hat is approximately given by

$$F_{\rm eff}(a, R_{\rm TH}, \rho_{\rm TH}, \rho_{\rm env}) = \frac{1}{3}\left[3\left(\frac{\Delta R}{R_{\rm TH}}\right) - 3\left(\frac{\Delta R}{R_{\rm TH}}\right)^2 + \left(\frac{\Delta R}{R_{\rm TH}}\right)^3\right] \tag{A.3a}$$

$$\frac{\Delta R}{R_{\rm TH}} = \min\left\{\frac{3|f_{\mathcal{R}}^{\rm TH} - f_{\mathcal{R}}^{\rm env}|}{2\Phi_N}, 1\right\} \tag{A.3b}$$

and $f_{\mathcal{R}}^{\rm TH} = f_{\mathcal{R}}(\rho_{\rm TH})$ and $f_{\mathcal{R}}^{\rm env} = f_{\mathcal{R}}(\rho_{\rm env})$ are the scalar field values inside and outside the body respectively. When the over-density is massive or is located in a very dense environment then $\frac{\Delta R}{R_{\rm TH}} \ll 1$ and the fifth-force is screened. In contrast, when the over-density is not massive, then $\frac{\Delta R}{R_{\rm TH}} \approx 1$ and the force is 4/3 the value of the Newtonian prediction. This completes our discussion of $f(\mathcal{R})$.

A.2 Symmetron gravity

The symmetron mechanism adds to ΛCDM a scalar field with an artificially-imposed $\mathbb{Z}_2$ symmetry and a coupling to matter [18, 27, 65]. The breaking of this symmetry occurs when the environmental density drops below a critical value, which causes the matter-scalar coupling to become non-zero [18].

The free parameters in our model are [66]:

1. The range of the field at which $\rho = 0$ in Mpc/h : $\lambda_0 = \frac{1}{\mu\sqrt{2}}$
2. A dimensionless coupling constant $\beta_0 = \phi_0 \frac{M_{Pl}}{M_0} = \frac{\mu}{\sqrt{\lambda}} \frac{M_{Pl}}{M_0}$
3. The scale factor at which the background density takes the value required for symmetry breaking in the cosmological background $a_{SSB} = \frac{\rho_0}{\mu^2 M_0^2}$

We set $\lambda_0 = 1$, $\beta_0 = 1$ and $a_{SSB} = 0.33$, 0.5 in our simulations.

The effective gravitational potential can be expressed similarly to that of $f(\mathcal{R})$. The scalar field value in the cosmological background and inside the halo are:

$$F_{\rm env} = \sqrt{1 - \left(\frac{a_{\rm SSB}}{a}\right)^3} \tag{A.4a}$$

$$F_h = \sqrt{1 - (1+\delta) a_{\rm SSB}^3)} \tag{A.4b}$$

which leads to a thin-shell factor

$$\frac{\Delta R}{R_{\rm TH}} = \frac{\Omega_{m0}}{a_{\rm SSB}^3} \frac{\lambda_0^2}{\Phi_N} \frac{|F_h - F_{\rm env}|}{F_{\rm env}} \tag{A.4c}$$

and as per $f(\mathcal{R})$ the effective factor is:

$$F_{\rm eff} = 2\left(\beta_0 F_{\rm env}\right)^2 \min\left\{3\frac{\Delta R}{R_{\rm TH}}, 1\right\} \tag{A.4d}$$

By analogy with the chameleon potential in Appendix A.1, the modification falls into an unscreened regime where $\phi_{\rm in} \approx \phi_0$ and the scalar field cannot relax to the value at the effective minimum of the potential $V(\phi)$; and a screened regime where $\phi_{\rm in}$ is suppressed exponentially compared to ϕ_0. Thus, we see that despite the different mechanism by which screening occurs, the result is very similar for both the chameleon screening in $f(\mathcal{R})$ gravity and symmetron gravity.

A.3 DGP gravity

Dvali-Gabadadze-Porrati (DGP) gravity is a braneworld model, in which the usual $(3+1)$ foliated hypersurfaces are a brane embedded in a(n otherwise empty) higher-dimensional spacetime known as the bulk. While the Standard Model interactions are limited to the brane, gravitational interactions extend into the bulk. The DGP model employs Vainshtein screening to remain observationally viable.

Dvali-Gabadadze-Porrati gravity embeds the FLRW manifold into a 5D Minkowski manifold, where the free parameter is the crossover scale:

$$r_c \equiv \frac{{}^{(5\mathrm{D})}\kappa}{2^{(4\mathrm{D})}\kappa} \quad \text{where } {}^{(4\mathrm{D})}\kappa = (8\pi G_N) \text{ as usual} \tag{A.5}$$

On scales $r \gg r_c$, the 5D effects are unscreened, whereas on scales $r \ll r_c$, the brane is unaffected by the presence of the bulk and the dynamics are screened [67].

In the weak-field, quasi-static limit, the equation of motion for the scalar field and the equations for the potentials can be combined to obtain a modified Poission equation with:

$$F_{\text{eff}}(r,a) = \frac{2}{3\beta(a)} \frac{\sqrt{1+x^{-3}}-1}{x^{-3}} \quad \text{where } x(r,a) \equiv \frac{r}{R_*} \tag{A.6}$$

where R_* is the Vainshtein radius for the mass $M(r)$ enclosed inside the radius r

$$R_*(r,a) = \left(r_c^2 \frac{16c^2 G_N \delta M(r)}{9\beta^2(a)} \right)^{\frac{1}{3}} \tag{A.7a}$$

where we define

$$\beta(\phi) \equiv 1 + 2r_c H(a) \left(1 + \frac{\dot{H}(a)}{3H^2(a)} \right) \tag{A.7b}$$

The scalar field is unscreeened outside the Vainshtein radius and screened within it. This completes our discussion of DGP gravity.

B Calibration of Multinest

We used the `MultiNest` nested sampling algorithm of [59] to carry out the integrals in the previous subsections. This section describes the calibration process we used to tune the algorithm.

The simulated data in this section was made by generating an HMF with the "default" parameter values for each fitting function, i.e. the values in the original publication. The Poisson error was simulated by scattering each data point by a value in $[-\sqrt{N}, \sqrt{N}]$, where N is the number of haloes per bin. We used 10, 30 and 100 data points, equivalent to binning our halo data into equal-ln M bins. (Recall that the number of bins suggested by the optimisation in Section 4.3 was ~ 30.) The `MultiNest` parameters were selected until both the Poisson and Gaussian likelihoods returned credible regions which included the original parameter.

The key settings are tabulated in Table 5.

Description	Values tested	Final value
Importance Nested Sampling	True, False	True
Identify multi-modal posteriors	True, False	False
Number of live points	100 200 500 1000	500
Tolerance factor	1d-4, 5d-4, 5d-3, 5d-2, 5d-1	1d-4
Sampling efficiency	3d-1, 5d-1, 8d-1, 1, 2	8d-1

Table 5: Calibration parameters used to tune `MultiNest`. The same values were used for both likelihood functions.

Now we analyse the effect of the bin width, the number of live points and the choice of likelihood function on simulated data. We discussed the simulated data in Section 5.3. Having calibrated `MultiNest`, the algorithm was used to recover (as best as possible) the input parameter values. The properties which we varied were:

1. The likelihood function: Gaussian or Poissonian
2. The number of live points
3. The number of bins: 10, 30 or 100 (equivalently, the bin width)

Figures 9 to 14 show—for a given HMF—the posteriors produced by the Poissonian likelihood functions. The number of live points is indicated by the colour of the credible regions. The dashed black line shows the value of the parameter at input.

The choice of likelihood function has a common behaviour across all of the HMFs: that the Poissonian likelihood is superior to both the Gaussian ones. We do not show posterior figures for the Gaussian data here because we found that the Gaussian likelihood produces broad rather than peaked posteriors—in fact the 1σ regions occupy most of the parameter space. Expanding the prior volume did not affect this result, which indicates that the posteriors are prior driven rather than constrained by the data. The credible regions do not shrink appreciably when the number of live points is dramatically increased (from 10^1 to 10^4), so this is a consequence of the likelihood rather than the algorithm used to calculate it. Moreover, this is not a consequence of the scatter in the data, because the Poisson likelihood

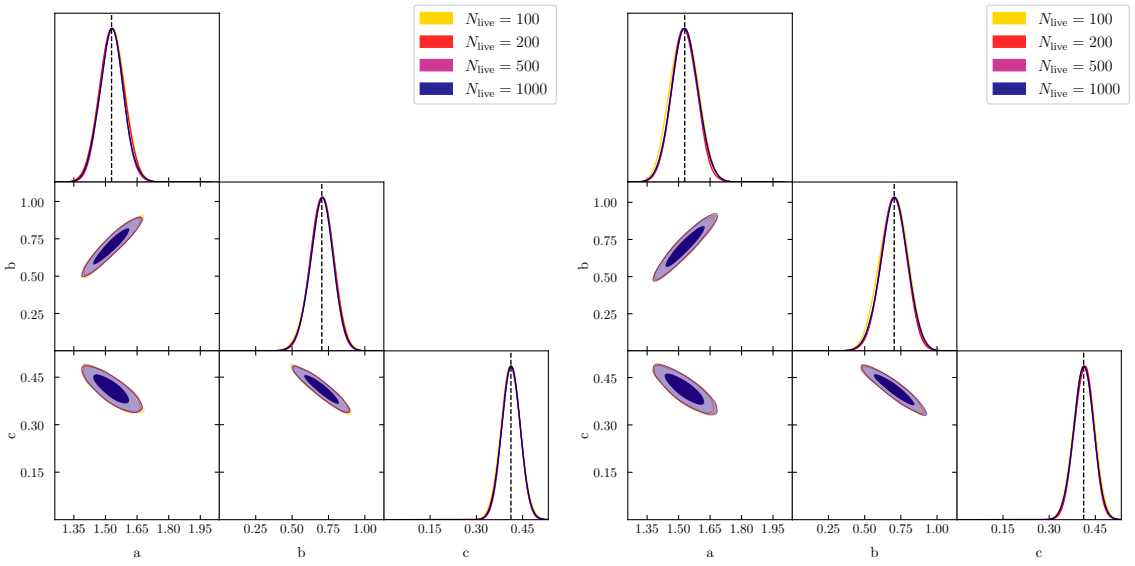

(a) lenm = 10

(b) lenm = 30

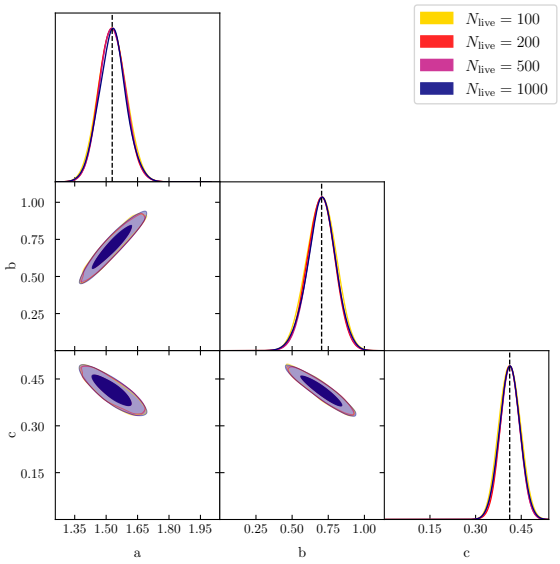

(c) lenm = 100

Figure 9: The effect of changing bin width on the Peacock HMF. The triangle plot is the same as Figure 11. The subfigure captions show the number of bins used in calculating the input HMF and discretising the model HMFs proposed by the nested sampling routine.

does produce narrow, peaked posteriors with the same data. We find that these trends are independent of the bin width used. The only way to utilise the Gaussian likelihood is to replace the Poisson errors with much smaller ones. For example, [2] run multiple N-body simulations and use jack-knife errors which are much smaller. However, it is impractical to replicate this in the synthesised data. Therefore we do not apply the Gaussian likelihood

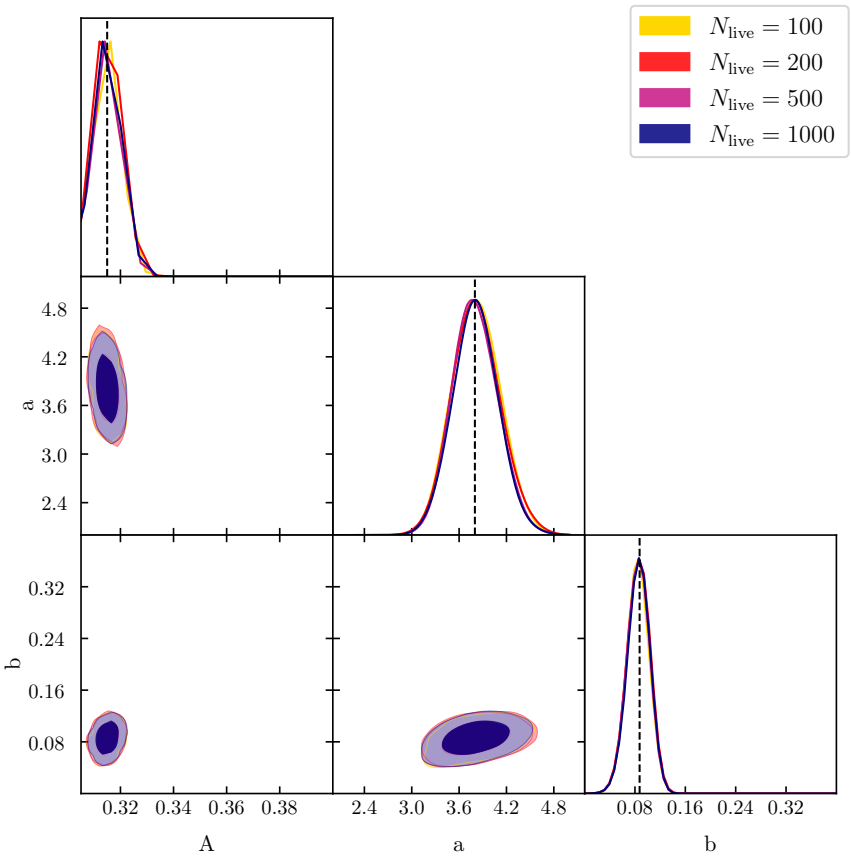

Figure 10: Posteriors for the Jenkins HMF using different numbers of live points (coloured). The main diagonal shows the 1-d posteriors marginalised over all other parameters, while the off-diagonal plots show correlations between pairs of parameters via the 2-d $1, 2\sigma$ credible regions. The black dashed lines show the input values, while the coloured lines show the PDF of the values recovered by nested sampling, with 30 bins, assuming a Poissonian likelihood.

to our halo data. This illustrates the importance of correctly selecting a likelihood function using maximum entropy principles (i.e. based upon the underlying distribution in the data).

The number of live points is of interest as we need to find a compromise between efficiency and accuracy. The higher the dimensionality of the parameter space, the more live points are typically required to constrain the posterior. However, we find that once the number is increased beyond 10^2, there is usually little difference between the 100, 200, 500 and 1000 posteriors. (`MultiNest` advises using fewer than 1000 live points when the Importance Nested Sampling mode is used, due to memory constraints.) The credible regions all largely overlap, indepedent of the number of live points. The marginalised posteriors usually overlap as well (e.g. all parameters in Figures 10 and 11; $\{A, a\}$ in Figure 12; $\{A, b, c\}$ in Figure 14). In some cases (p in Figure 12; a in Figure 14) the peaks of the posteriors move further from or closer to the original value. This does not affect the result that in all cases the input parameters lie within the 1-σ credible regions. This illustrates the need to find a minimum number of live points for which the results converge and ensuring that adding more live points does not move the ML and MAP estimates outside the existing credible regions. This

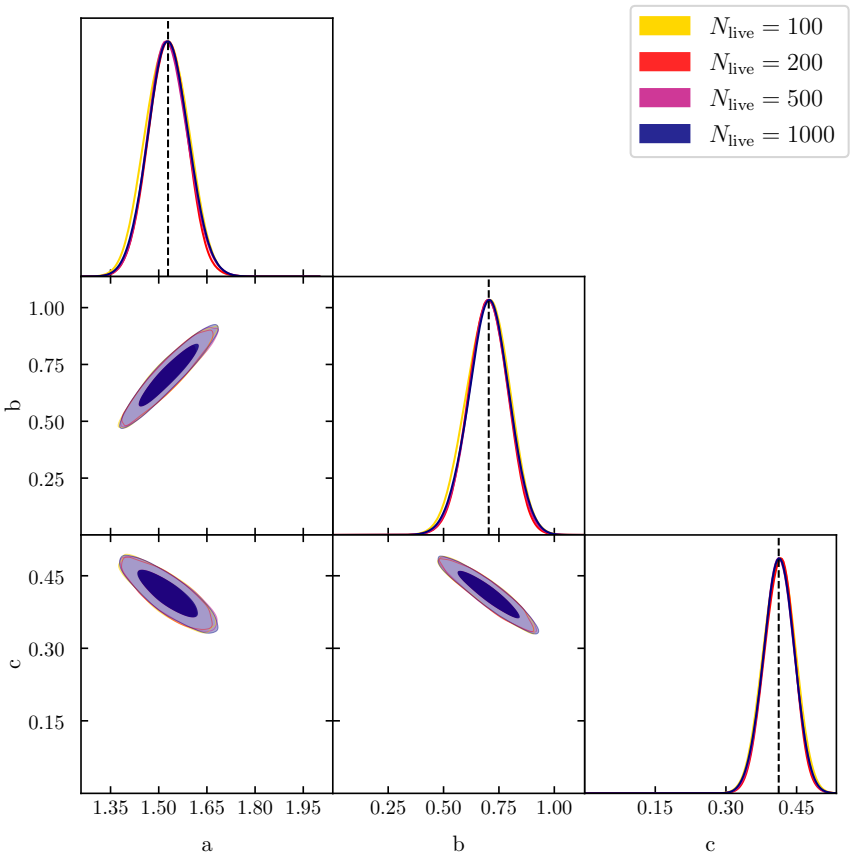

Figure 11: Posteriors for the Peacock HMF using different numbers of live points (coloured). The main diagonal shows the 1-d posteriors marginalised over all other parameters, while the off-diagonal plots show correlations between pairs of parameters via the 2-d $1, 2\sigma$ credible regions. The black dashed lines show the input values, while the coloured lines show the PDF of the values recovered by nested sampling, with 30 bins, assuming a Poissonian likelihood.

demonstrates that our estimates of the posteriors have already converged to an accurate representation of the likelihood with only $\sim 10^2$ live points.

The number of bins is a compromise between the amount of information provided by the data and the scatter in this information. Thinner bins produce more data points with which to constrain the parameter values, so we expect smaller credible regions with 100 than with 30 bins. However, the finite number of haloes in the simulation limit the number of samples drawn from the continuous (underlying) distribution (which would be obtained with an infinite number of haloes as the bin width approached zero). Therefore—particularly at the high-mass end with few haloes—bins may be insufficiently wide to preserve the monotonicity of the HMF, or may be empty altogether. This does not only widen the posteriors, but may also shift the peaks, if the low-mass end does not provide sufficient constraints where the scatter is minimal. In our simulated "data," we have maximised the scatter (to within Poisson errors) to produce a pessimistic scenario. The performance of each HMF is similar, so we only show the Peacock HMF in Figure 9. We find that this produces little to no effect on the location or width of the 1σ credible regions. This behaviour is largely independent of

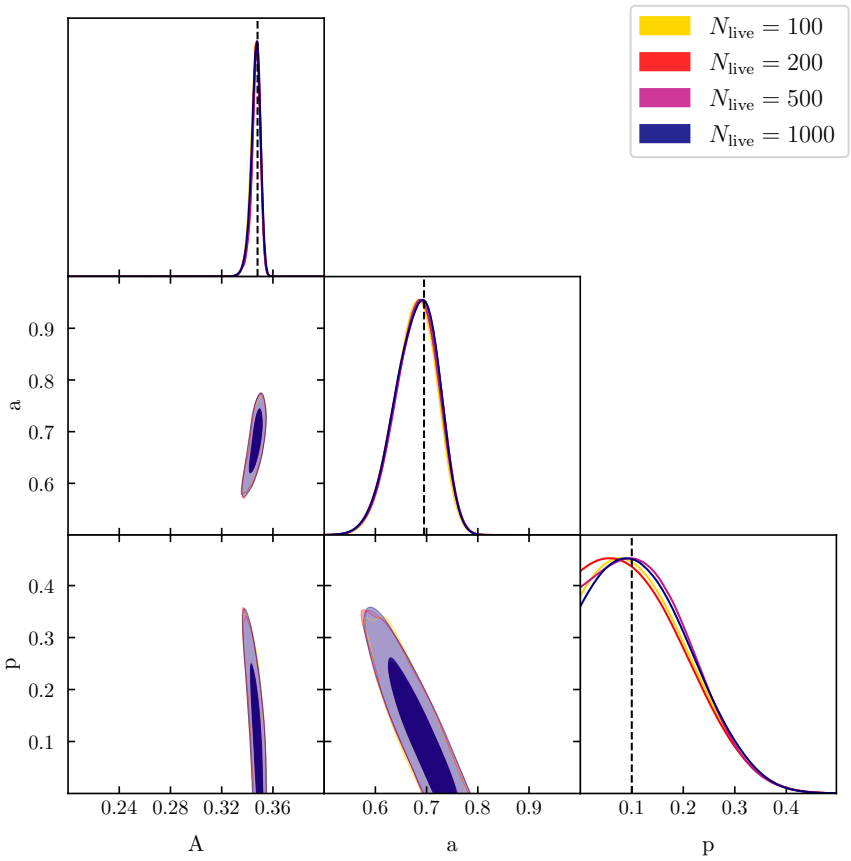

Figure 12: Posteriors for the SMT-Courtin HMF using different numbers of live points (coloured). The main diagonal shows the 1-d posteriors marginalised over all other parameters, while the off-diagonal plots show correlations between pairs of parameters via the 2-d $1, 2\sigma$ credible regions. The black dashed lines show the input values, while the coloured lines show the PDF of the values recovered by nested sampling, with 30 bins, assuming a Poissonian likelihood.

the number of live points as well.

Finally we examine the effect of the number of free parameters. The HMFs with three free parameters—Jenkins, Peacock and SMT-Courtin—can all be reasonably constrained by the available data. Of the two four-parameter fits, Warren-Crocce also recovers the required values whereas Tinker-Angulo-Watson does not produce such an accurate result. Although `MultiNest` did find the ML values to within a few percent of the input values, the posteriors created by `GetDist` showed a broad tail in its credible regions for $\{A, a, b\}$, while c was fine. Although the chains do converge as we increase the number of live points, they converge to the wrong values when examining the peaks in the posterior (as processed by `GetDist`). The nested sampling ellipses exclude the ML value at some point during the sampling, from which point onwards the sample can only be drawn from within the likelihood iso-surface created by the ellipses. (This is hardly surprising given that $A(b\nu)^a$ is automatically degenerate. Such behaviour was also seen in [68].) The Reed 2007 fit has six parameters. In this case the Poissonian likelihood cannot identify the original parameter values used to create the data.

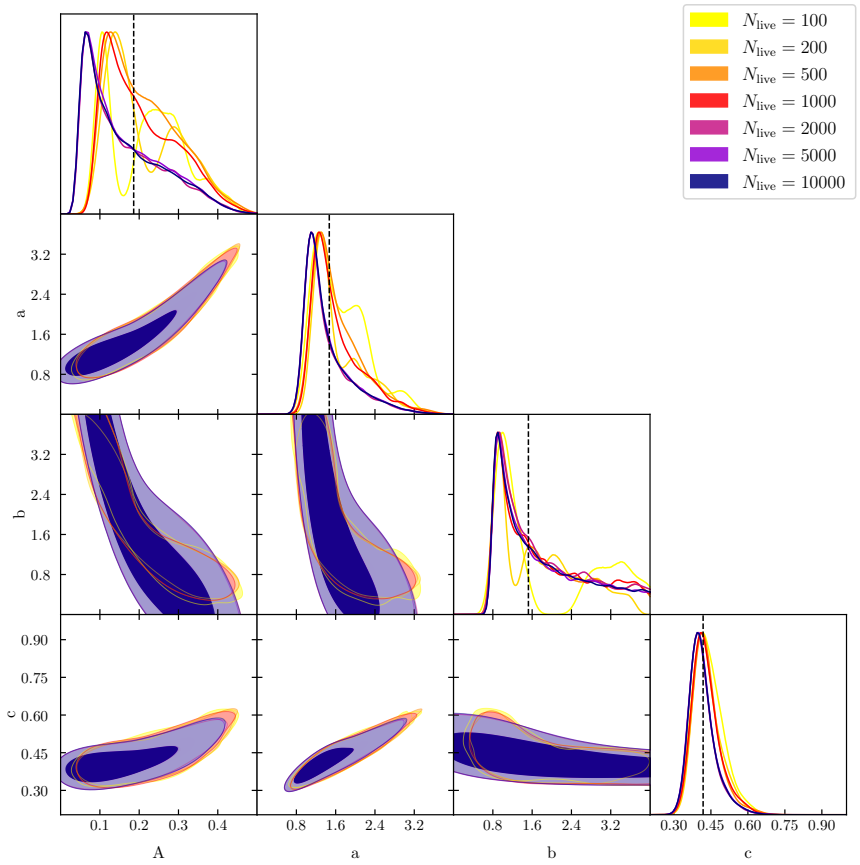

Figure 13: Posteriors for the Tinker-Angulo-Watson HMF using different numbers of live points (coloured). The main diagonal shows the 1-d posteriors marginalised over all other parameters, while the off-diagonal plots show correlations between pairs of parameters via the 2-d $1, 2\sigma$ credible regions. The black dashed lines show the input values, while the coloured lines show the PDF of the values recovered by nested sampling, with 30 bins, assuming a Poissonian likelihood.

Many pairs of parameters in this fitting function are degenerate (Table 4). This may be a failure of the data as well: counts must be rounded to an integer value (to correspond with the behaviour in our N-body derived data) and, once scattered, could be negative. Rounding the counts mapped a small portion of the parameter space (used for calculating the first-crossing distribution) to the same counts. The two factors which affect this conversion are the box size and the bin width (larger boxes create more haloes; wider bins include more haloes). The behaviour of the fit agrees with statements in [12, 14] that some of their parameters can only be constrained by masses $M \geq 10^{15} M_{\odot}$, of which we have very few in the halo data. The nested sampling algorithm is not infallible. For this reason, we exclude the Reed and Tinker-Angulo-Watson fits from our halo results in the next two sections.

Having explored the effects of the likelihood function, the number of bins and the number of live points, we have found that the optimal choices are the Poissonian likelihood function with at least 100 live points and that the number of bins is irrelevant. Thus we set 30 bins and 500 live points for our data proper in the next two sections. We also exclude

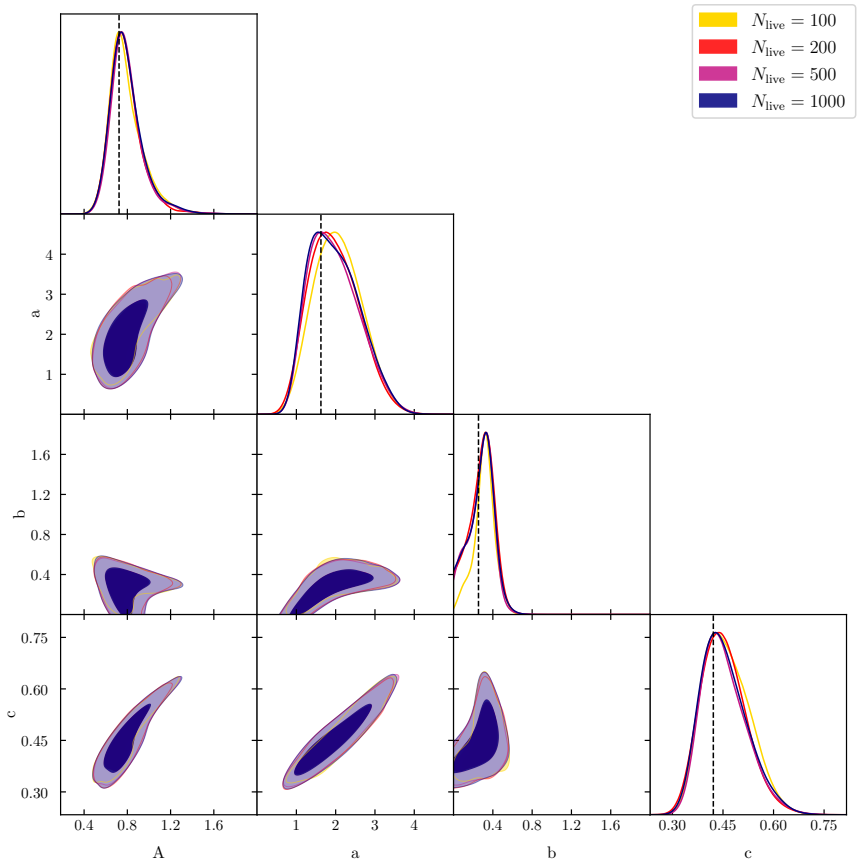

Figure 14: Posteriors for the Warren-Crocce HMF using different numbers of live points (coloured). The main diagonal shows the 1-d posteriors marginalised over all other parameters, while the off-diagonal plots show correlations between pairs of parameters via the 2-d $1, 2\sigma$ credible regions. The black dashed lines show the input values, while the coloured lines show the PDF of the values recovered by nested sampling, with 30 bins, assuming a Poissonian likelihood.

the Tinker-Angulo-Watson and Reed-07 fits on the basis that we have insufficient data to properly constrain their free parameters.

References

[1] A. R. Zentner, *The Excursion Set Theory of Halo Mass Functions, Halo Clustering, and Halo Growth*, *Int.J.Mod.Phys.* **D16** (2007) 763–816, [astro-ph/0611454].

[2] A. J. Benson, *The mass function of unprocessed dark matter haloes and merger tree branching rates*, *MNRAS* **467** (May, 2017) 3454–3466, [arXiv:1610.0105].

[3] S. Bhattacharya, K. Heitmann, M. White, Z. Lukić, C. Wagner, and S. Habib, *Mass Function Predictions Beyond ΛCDM*, *Astrophysical Journal* **732** (May, 2011) 122, [arXiv:1005.2239].

[4] T. Clifton, P. G. Ferreira, A. Padilla, and C. Skordis, *Modified Gravity and Cosmology*, *Phys.Rept.* **513** (2012) 1–189, [arXiv:1106.2476].

[5] P. Bull, Y. Akrami, J. Adamek, T. Baker, E. Bellini, J. Beltrán Jiménez, E. Bentivegna, S. Camera, S. Clesse, J. H. Davis, E. Di Dio, J. Enander, A. Heavens, L. Heisenberg, B. Hu, C. Llinares, R. Maartens, E. Mörtsell, S. Nadathur, J. Noller, R. Pasechnik, M. S. Pawlowski, T. S. Pereira, M. Quartin, A. Ricciardone, S. Riemer-Sørensen, M. Rinaldi, J. Sakstein, I. D. Saltas, V. Salzano, I. Sawicki, A. R. Solomon, D. Spolyar, G. D. Starkman, D. Steer, I. Tereno, L. Verde, F. Villaescusa-Navarro, M. von Strauss, and H. A. Winther, *Beyond Λ CDM: Problems, solutions, and the road ahead*, *Physics of the Dark Universe* **12** (June, 2016) 56–99, [arXiv:1512.0535].

[6] Planck Collaboration, P. A. R. Ade, N. Aghanim, M. Arnaud, M. Ashdown, J. Aumont, C. Baccigalupi, A. J. Banday, R. B. Barreiro, J. G. Bartlett, and et al., *Planck 2015 results. XIII. Cosmological parameters*, *A&A* **594** (Sept., 2016) A13, [arXiv:1502.0158].

[7] W. H. Press and P. Schechter, *Formation of Galaxies and Clusters of Galaxies by Self-Similar Gravitational Condensation*, *Astrophysical Journal* **187** (Feb., 1974) 425–438.

[8] S. G. Murray, C. Power, and A. S. G. Robotham, *HMFcalc: An online tool for calculating dark matter halo mass functions*, *Astronomy and Computing* **3** (Nov., 2013) 23–34, [arXiv:1306.6721].

[9] J. Tinker, A. V. Kravtsov, A. Klypin, K. Abazajian, M. Warren, G. Yepes, S. Gottlöber, and D. E. Holz, *Toward a Halo Mass Function for Precision Cosmology: The Limits of Universality*, *Astrophysical Journal* **688** (Dec., 2008) 709–728, [arXiv:0803.2706].

[10] E. Juan, E. Salvador-Solé, G. Domènech, and A. Manrique, *Halo mass definition and multiplicity function*, *MNRAS* **439** (Apr., 2014) 3156–3167, [arXiv:1401.7334].

[11] Z. Lukić, K. Heitmann, S. Habib, S. Bashinsky, and P. M. Ricker, *The Halo Mass Function: High-Redshift Evolution and Universality*, *Astrophysical Journal* **671** (Dec., 2007) 1160–1181, [astro-ph/0702360].

[12] D. S. Reed, R. Bower, C. S. Frenk, A. Jenkins, and T. Theuns, *The halo mass function from the dark ages through the present day*, *MNRAS* **374** (Jan., 2007) 2–15, [astro-ph/0607150].

[13] M. S. Warren, K. Abazajian, D. E. Holz, and L. Teodoro, *Precision Determination of the Mass Function of Dark Matter Halos*, *Astrophysical Journal* **646** (Aug., 2006) 881–885, [astro-ph/0506395].

[14] D. Reed, J. Gardner, T. Quinn, J. Stadel, M. Fardal, G. Lake, and F. Governato, *Evolution of the mass function of dark matter haloes*, *MNRAS* **346** (Dec., 2003) 565–572, [astro-ph/0301270].

[15] G. Despali, C. Giocoli, R. E. Angulo, G. Tormen, R. K. Sheth, G. Baso, and L. Moscardini, *The universality of the virial halo mass function and models for non-universality of other halo definitions*, *MNRAS* **456** (2016), no. 3 2486–2504, [arXiv:1507.0562].

[16] J. Courtin, Y. Rasera, J.-M. Alimi, P.-S. Corasaniti, V. Boucher, and A. Füzfa, *Imprints of*

dark energy on cosmic structure formation - II. Non-universality of the halo mass function, *MNRAS* **410** (Jan., 2011) 1911–1931, [arXiv:1001.3425].

[17] F. von Braun-Bates, H. A. Winther, D. Alonso, and J. Devriendt, *The $f(R)$ halo mass function in the cosmic web*, *JCAP* **3** (Mar., 2017) 012, [arXiv:1702.0681].

[18] L. Taddei, R. Catena, and M. Pietroni, *Spherical collapse and halo mass function in the symmetron model*, *Physical Review D* **89** (Jan., 2014) 023523, [arXiv:1310.6175].

[19] L. Lombriser, B. Li, K. Koyama, and G.-B. Zhao, *Modeling halo mass functions in chameleon f(R) gravity*, *Phys.Rev.* **D87** (2013), no. 12 123511, [arXiv:1304.6395].

[20] F. Schmidt, W. Hu, and M. Lima, *Spherical collapse and the halo model in braneworld gravity*, *Physical Review D* **81** (Mar., 2010) 063005, [arXiv:0911.5178].

[21] A. Barreira, B. Li, C. M. Baugh, and S. Pascoli, *Spherical collapse in Galileon gravity: fifth force solutions, halo mass function and halo bias*, *JCAP* **11** (Nov., 2013) 056, [arXiv:1308.3699].

[22] M. Kopp, S. A. Appleby, I. Achitouv, and J. Weller, *Spherical collapse and halo mass function in $f(R)$ theories*, *Phys.Rev.* **D88** (2013), no. 8 084015, [arXiv:1306.3233].

[23] Y. Li and W. Hu, *Chameleon halo modeling in f(R) gravity*, *Physical Review D* **84** (Oct., 2011) 084033, [arXiv:1107.5120].

[24] A. Barreira, B. Li, W. A. Hellwing, C. M. Baugh, and S. Pascoli, *Nonlinear structure formation in the cubic Galileon gravity model*, *JCAP* **10** (Oct., 2013) 027, [arXiv:1306.3219].

[25] A. Barreira, B. Li, W. A. Hellwing, L. Lombriser, C. M. Baugh, and S. Pascoli, *Halo model and halo properties in Galileon gravity cosmologies*, *JCAP* **4** (Apr., 2014) 029, [arXiv:1401.1497].

[26] J. Khoury and A. Weltman, *Chameleon cosmology*, *Phys.Rev.* **D69** (2004) 044026, [astro-ph/0309411].

[27] K. Hinterbichler and J. Khoury, *Screening Long-Range Forces through Local Symmetry Restoration*, *Physical Review Letters* **104** (June, 2010) 231301, [arXiv:1001.4525].

[28] K. Hinterbichler, J. Khoury, A. Levy, and A. Matas, *Symmetron cosmology*, *Physical Review D* **84** (Nov., 2011) 103521, [arXiv:1107.2112].

[29] A. I. Vainshtein, *To the problem of nonvanishing gravitation mass*, *Phys. Lett.* **39B** (1972) 393–394.

[30] W. Hu and I. Sawicki, *Models of f(R) Cosmic Acceleration that Evade Solar-System Tests*, *Phys.Rev.* **D76** (2007) 064004, [arXiv:0705.1158].

[31] G. Dvali, G. Gabadadze, and M. Porrati, *4D gravity on a brane in 5D Minkowski space*, *Physics Letters B* **485** (July, 2000) 208–214, [hep-th/0005016].

[32] A. de Felice, T. Kobayashi, and S. Tsujikawa, *Effective gravitational couplings for cosmological perturbations in the most general scalar-tensor theories with second-order field equations*, *Physics Letters B* **706** (Dec., 2011) 123–133, [arXiv:1108.4242].

[33] E. Berti, E. Barausse, V. Cardoso, L. Gualtieri, P. Pani, U. Sperhake, L. C. Stein, N. Wex, K. Yagi, T. Baker, C. P. Burgess, F. S. Coelho, D. Doneva, A. De Felice, P. G. Ferreira, P. C. C. Freire, J. Healy, C. Herdeiro, M. Horbatsch, B. Kleihaus, A. Klein, K. Kokkotas, J. Kunz, P. Laguna, R. N. Lang, T. G. F. Li, T. Littenberg, A. Matas, S. Mirshekari, H. Okawa, E. Radu, R. O'Shaughnessy, B. S. Sathyaprakash, C. Van Den Broeck, H. A. Winther, H. Witek, M. Emad Aghili, J. Alsing, B. Bolen, L. Bombelli, S. Caudill, L. Chen, J. C. Degollado, R. Fujita, C. Gao, D. Gerosa, S. Kamali, H. O. Silva, J. G. Rosa, L. Sadeghian, M. Sampaio, H. Sotani, and M. Zilhao, *Testing general relativity with present and future astrophysical observations*, *Classical and Quantum Gravity* **32** (Dec., 2015) 243001, [arXiv:1501.0727].

[34] B. Li and G. Efstathiou, *An extended excursion set approach to structure formation in chameleon models*, *Mon.Not.Roy.Astron.Soc.* **421** (Apr., 2012) 1431–1442, [arXiv:1110.6440].

[35] R. K. Sheth, H. J. Mo, and G. Tormen, *Ellipsoidal collapse and an improved model for the number and spatial distribution of dark matter haloes*, *MNRAS* **323** (May, 2001) 1–12, [astro-ph/9907024].

[36] R. K. Sheth and G. Tormen, *An Excursion set model of hierarchical clustering : Ellipsoidal collapse and the moving barrier*, *Mon.Not.Roy.Astron.Soc.* **329** (2002) 61, [astro-ph/0105113].

[37] M. Maggiore and A. Riotto, *The Halo mass function from excursion set theory. III. Non-Gaussian fluctuations*, *Astrophys. J.* **717** (2010) 526–541, [arXiv:0903.1251].

[38] A. Jenkins, C. S. Frenk, S. D. M. White, J. M. Colberg, S. Cole, A. E. Evrard, H. M. P. Couchman, and N. Yoshida, *The mass function of dark matter haloes*, *MNRAS* **321** (Feb., 2001) 372–384, [astro-ph/0005260].

[39] M. Cataneo, D. Rapetti, L. Lombriser, and B. Li, *Cluster abundance in chameleon f(R) gravity I: toward an accurate halo mass function prediction*, *JCAP* **12** (Dec., 2016) 024, [arXiv:1607.0878].

[40] J. A. Peacock, *Testing anthropic predictions for Λ and the cosmic microwave background temperature*, *MNRAS* **379** (Aug., 2007) 1067–1074, [arXiv:0705.0898].

[41] M. Crocce, P. Fosalba, F. J. Castander, and E. Gaztañaga, *Simulating the Universe with MICE: the abundance of massive clusters*, *MNRAS* **403** (Apr., 2010) 1353–1367, [arXiv:0907.0019].

[42] K. Parfrey, L. Hui, and R. K. Sheth, *Scale-dependent halo bias from scale-dependent growth*, *Physical Review D* **83** (Mar., 2011) 063511, [arXiv:1012.1335].

[43] J. Zhang and L. Hui, *On random walks with a general moving barrier*, *Astrophys. J.* **641** (2006) 641–646, [astro-ph/0508384].

[44] J. R. Bond, S. Cole, G. Efstathiou, and N. Kaiser, *Excursion set mass functions for hierarchical Gaussian fluctuations*, *Astrophysical Journal* **379** (Oct., 1991) 440–460.

[45] B. Li and T. Y. Lam, *Excursion set theory for modified gravity: Eulerian versus Lagrangian environments*, *MNRAS* **425** (Sept., 2012) 730–739, [arXiv:1205.0058].

[46] R. E. Angulo, V. Springel, S. D. M. White, A. Jenkins, C. M. Baugh, and C. S. Frenk, *Scaling relations for galaxy clusters in the Millennium-XXL simulation*, *MNRAS* **426** (Nov., 2012) 2046–2062, [arXiv:1203.3216].

[47] W. A. Watson, I. T. Iliev, A. D'Aloisio, A. Knebe, P. R. Shapiro, and G. Yepes, *The halo mass function through the cosmic ages*, *MNRAS* **433** (Aug., 2013) 1230–1245, [arXiv:1212.0095].

[48] C. Llinares, D. F. Mota, and H. A. Winther, *ISIS: a new N-body cosmological code with scalar fields based on RAMSES. Code presentation and application to the shapes of clusters*, *A&A* **562** (Feb., 2014) A78, [arXiv:1307.6748].

[49] B. Li, G.-B. Zhao, R. Teyssier, and K. Koyama, *ECOSMOG: an Efficient COde for Simulating MOdified Gravity*, *JCAP* **1** (Jan., 2012) 051, [arXiv:1110.1379].

[50] R. Teyssier, *Cosmological hydrodynamics with adaptive mesh refinement. A new high resolution code called RAMSES*, *A&A* **385** (Apr., 2002) 337–364, [astro-ph/0111367].

[51] H. A. Winther, F. Schmidt, A. Barreira, C. Arnold, S. Bose, C. Llinares, M. Baldi, B. Falck, W. A. Hellwing, K. Koyama, B. Li, D. F. Mota, E. Puchwein, R. E. Smith, and G.-B. Zhao, *Modified gravity N-body code comparison project*, *MNRAS* **454** (Dec., 2015) 4208–4234, [arXiv:1506.0638].

[52] P. Brax, A.-C. Davis, B. Li, H. A. Winther, and G.-B. Zhao, *Systematic simulations of modified gravity: symmetron and dilaton models*, *JCAP* **10** (Oct., 2012) 002, [arXiv:1206.3568].

[53] P. S. Behroozi, R. H. Wechsler, and H.-Y. Wu, *The ROCKSTAR Phase-space Temporal Halo Finder and the Velocity Offsets of Cluster Cores*, *Astrophysical Journal* **762** (Jan., 2013) 109, [arXiv:1110.4372].

[54] M. Davis, G. Efstathiou, C. S. Frenk, and S. D. M. White, *The evolution of large-scale structure in a universe dominated by cold dark matter*, *Astrophysical Journal* **292** (May, 1985) 371–394.

[55] A. Knebe, S. R. Knollmann, S. I. Muldrew, F. R. Pearce, M. A. Aragon-Calvo, Y. Ascasibar, P. S. Behroozi, D. Ceverino, S. Colombi, J. Diemand, K. Dolag, B. L. Falck, P. Fasel, J. Gardner, S. Gottlöber, C.-H. Hsu, F. Iannuzzi, A. Klypin, Z. Lukić, M. Maciejewski, C. McBride, M. C. Neyrinck, S. Planelles, D. Potter, V. Quilis, Y. Rasera, J. I. Read, P. M. Ricker, F. Roy, V. Springel, J. Stadel, G. Stinson, P. M. Sutter, V. Turchaninov, D. Tweed, G. Yepes, and M. Zemp, *Haloes gone MAD: The Halo-Finder Comparison Project*, *MNRAS* **415** (Aug., 2011) 2293–2318, [arXiv:1104.0949].

[56] D. Freedman and P. Diaconis, *On the histogram as a density estimator:l 2 theory*, *Zeitschrift fur Wahrscheinlichkeitstheorie und Verwandte Gebiete* **57** (dec, 1981) 453–476.

[57] K. H. Knuth, *Optimal Data-Based Binning for Histograms*, *ArXiv Physics e-prints* (May, 2006) [physics/0605197].

[58] R. Barlow, *Asymmetric Statistical Errors*, *ArXiv Physics e-prints* (June, 2004) [physics/0406120].

[59] F. Feroz, M. P. Hobson, and M. Bridges, *MULTINEST: an efficient and robust Bayesian inference tool for cosmology and particle physics*, *MNRAS* **398** (Oct., 2009) 1601–1614, [arXiv:0809.3437].

[60] D. Alonso, E. Eardley, and J. A. Peacock, *Halo abundances within the cosmic web*, *Mon.Not.Roy.Astron.Soc.* **447** (2015) 2683, [arXiv:1406.4159].

[61] G. Efstathiou, *An anthropic argument for a cosmological constant*, *MNRAS* **274** (June, 1995) L73–L76.

[62] J. Khoury and A. Weltman, *Chameleon cosmology*, *Phys.Rev.* **D69** (2004) 044026, [astro-ph/0309411].

[63] J. Khoury, *Theories of Dark Energy with Screening Mechanisms*, *ArXiv e-prints* (Nov., 2010) [arXiv:1011.5909].

[64] P. Brax, C. van de Bruck, A.-C. Davis, and D. J. Shaw, *f(R) gravity and chameleon theories*, *Physical Review D* **78** (Nov., 2008) 104021, [arXiv:0806.3415].

[65] M. Pietroni, *Dark energy condensation*, *Physical Review D* **72** (Aug., 2005) 043535, [astro-ph/0505615].

[66] H. A. Winther and P. G. Ferreira, *Fast route to nonlinear clustering statistics in modified gravity theories*, *Physical Review D* **91** (June, 2015) 123507, [arXiv:1403.6492].

[67] T. Clifton, *Cosmology without averaging*, *Classical and Quantum Gravity* **28** (2011), no. 16 164011.

[68] J. Buchner, *A statistical test for nested sampling algorithms*, *Statistics and Computing* **26** (sep, 2014) 383–392.